AMBIENT NOISE IN THE SURF ZONE

SARAH J. BASS

INFORMATION TO USERS

This manuscript has been reproduced from the microfilm master. UMI films the text directly from the original or copy submitted. Thus, some thesis and dissertation copies are in typewriter face, while others may be from any type of computer printer.

The quality of this reproduction is dependent upon the quality of the copy submitted. Broken or indistinct print, colored or poor quality illustrations and photographs, print bleedthrough, substandard margins, and improper alignment can adversely affect reproduction.

In the unlikely event that the author did not send UMI a complete manuscript and there are missing pages, these will be noted. Also, if unauthorized copyright material had to be removed, a note will indicate the deletion.

Oversize materials (e.g., maps, drawings, charts) are reproduced by sectioning the original, beginning at the upper left-hand corner and continuing from left to right in equal sections with small overlaps. Each original is also photographed in one exposure and is included in reduced form at the back of the book.

Photographs included in the original manuscript have been reproduced xerographically in this copy. Higher quality 6" x 9" black and white photographic prints are available for any photographs or illustrations appearing in this copy for an additional charge. Contact UMI directly to order.

UMI

A Bell & Howell Information Company
300 North Zeeb Road, Ann Arbor MI 48106-1346 USA
313/761-4700 800/521-0600

AMBIENT NOISE IN THE SURF ZONE

By

©Sarah J. Bass, B.Sc.

A thesis submitted to the School of Graduate

Studies in partial fulfillment of the

requirements for the degree of

Master of Science

Department of Physics

Memorial University of Newfoundland

November, 1995

St. John's Newfoundland Canada

Abstract

Ambient noise in the surf zone was recorded using a broad-band hydrophone, located approximately one meter below the sea surface, in the frequency range 100 Hz to 5 kHz. The predominant source of this noise is from breaking waves. Analysis of simultaneous land-based video observations of the sea surface in the region of the hydrophone, along with wave height data, reveals qualitative correlation between wave-breaking events and the hydrophone signal. In energetic surf, the sounds appear to be generated locally. Sounds from distant breaking events are not detected probably due to the effects of bubble screening. The detection by the hydrophone of breaking waves in the immediate vicinity implies that ambient noise in heavy surf provides a means of studying individual breakers and is a useful measure of local breaking frequency.

Contents

List of Figures

List of Tables

Acknowledgements

I would like to thank my supervisor, Dr. Alex Hay, for his guidance and for introducing me to Physical Oceanography. I am grateful to Wes Paul and Dr. Robert Craig for their help and for the many hours of work which provided the technical foundation of this research. Helpful discussions with Dr. Len Zedel, Dr. Brad de Young, and Doug Wilson are much appreciated. Financial support was provided by the Natural Sciences and Engineering Research Council of Canada.

On a personal note, I am grateful for my family's continual support, and for Jonathan, who lived through this with me.

Chapter 1

Introduction

1.1 Ambient Noise in the Ocean

Interest in oceanic ambient noise was first stimulated by Knudsen et al. (1948) who characterized the underwater sound near the ocean surface in terms of it's windspeed dependency and vertical directionality. It has long been known that the most important source of this sound, from a few hundred Hz to tens of kHz, is from breaking waves. Prompted by a desire to better understand this sound generation mechanism, many detailed theoretical and laboratory studies during the past 10 years have produced a plausible theory that centers on air bubbles entrained into the ocean through wave-breaking.

First suggested by Wenz (1962), the volume pulsations of individual bubbles are believed to be the major contributing mechanism to frequencies around several kilohertz (Medwin and Beaky, 1989). Even at low sea states, with little or no apparent white-capping, the sea surface sound appears to be dominated by bubble noise. Bubbles are excited into volume oscillations upon their formation either at the water surface or through fragmentation of larger bubbles. (Pumphrey and Ffowcs Williams, 1990). The oscillations then decay exponentially within milliseconds. Contributions of individual bubble oscillations to the acoustic radiation from laboratory spilling breakers has been studied by Medwin and Beaky (1989) and Medwin and Daniel (1990). Both recorded sound, radiated from individual bubbles at their formation, consistent with damped resonant air bubble theory. Updegraff and Anderson (1991) recorded similar signals about 1 m below the sea surface from gently spilling wind breakers. The acoustic record was interpreted as a superposition of individual bubble signatures. For the more energetic breakers, the creation of a larger number of bubbles meant that individual bubble sounds were not distinguishable. Whether this is the dominant source of sound in breaking waves was the subject of work by Banner and Cato (1988), who measured the sound from spilling breakers in a tank and recorded bubble entrainment using high-speed cinephotography. Their results indicate that the sound is emitted by bubbles on their initial formation at the surface or through

subsequent splitting or coalescence. They did not find any significant contribution to the acoustic record from bubble bursting or from non-spherical shape distortions. The sound assciated with the impact of droplets on the surface also appears to be negligible from the results of Pumphrey and Crum (1988). They studied the sound of a water droplet impacting on a water surface and found that the acoustic pressure level of the impact sound in the water was much smaller than that radiated by the oscillating bubble. Finally, the possibility of shape distortions, in the bubble, producing sound has been investigated theoretically by Longuet-Higgins (1990b) who has suggested a mechanism by which they may radiate at the same intensities observed for volume oscillations. This has not yet received strong support as a dominant sound generating source.

As noted by Prosperetti (1988a and 1988b), individual bubble oscillations, while conforming to theory, do not explain the broad maximum around 300-500 Hz in most ambient noise spectra. This frequency is significantly lower than the several kHz resonance frequency predicted for common bubble sizes in the ocean. Both Prosperetti, and Carey and Bradley (1985) independently proposed that a mechanism for this low frequency noise may be clouds of bubbles acting as a system of coupled oscillators and radiating at much lower frequencies than those of the individual bubbles of which the cloud is composed. The existence of these collective oscillations of a cloud of bubbles

have been confirmed in the laboratory by Kolaini et al. (1993) and Yoon et al. (1991).

Papanicolaou and Raichlen (1988) initiated the interest in cloud oscillations in relation to different types of breakers. They studied the acoustic emissions of laboratory plunging and spilling breakers and obtained significant high intensity low frequency signals for the case of the plunging breaker which did not occur for the spilling breaker case. They hypothesized that collective oscillations are the source of this low frequency sound, an idea supported by their video observations of cylindrical plumes created by the plunging breakers. The study of collective oscillations in laboratory breaking waves of varying intensities is taken further by Kolaini and Crum (1994) and Loewen and Melville (1994). In both studies, theoretical predictions of cloud oscillations, made with estimated cloud size and gas volume fraction, were in agreement with observed frequencies. Oguz (1994) also describes a theoretical model of low-frequency ambient noise levels generated by breaking wind waves. The sole sound source assumed in this model is that of collective oscillations from bubble clouds generated through wave breaking. Bubble clouds are described by bubble-size distribution, dipole strength of the entrained bubbles, void fraction, and cloud size distribution and growth. The noise levels predicted by Oguz are in good agreement with field measurements. These studies provide strong support for Prosperetti's model.

Recognizing that the nature of the radiated sound depends on the dynamics of the breaking wave, the acoustic signature may provide information as to the type of breaking wave and the energy dissipated in the process (Papanicolaou and Raichlen, 1988; Kolaini and Crum, 1994; Loewen and Melville, 1994). Many studies have also taken advantage of ambient noise to estimate and monitor ocean and wind conditions. (Farmer and Ding, 1992; Hollett, 1994; McConnell et al., 1992; Dupuis et al., 1993).

Ambient noise has been used to provide information on breaking wave distributions. Farmer and Vagle (1988a and 1988b) used a vertical array of hydrophones to record ambient noise at kilohertz frequencies in a water depth of 140 metres. The measurement depths were sufficiently close to the sea surface (1m, 10m, and 40m) to spatially filter the sound received at the hydrophones, based on a presumed dipole radiation from the breaking waves and the effects of absorption and spherical spreading. The reduction in the listening radius in this manner allowed the identification of individual breaking events. Farmer and Ding (1992) used a four-hydrophone array in the open ocean to locate and track individual breaking waves. Based on a model of underwater noise, Dupuis et al. (1993) studied the density and coverage of whitecaps through the variations in ambient noise. Ambient noise below 1500 Hz from a patch of sea surface with breaking waves was studied by Hollett (1994). Measurements were made with a vertical array of hydrophones in a water depth of 110 metres

and comparison made with a video recording of the patch of sea surface and wind speed observations. Discrete bursts of sound lasting a few seconds were associated with individual breaking waves occurring in the patch. Similar to the observations presented in this thesis. the source of these bursts is apparently generated in the breaking process.

Among the reports of field measurements of ambient noise. very few appear to have been concerned with studying the noise generated by breaking surf. Stewart (1994) and Wilson et al. (1985) both studied the effect of surf on ambient noise levels in shallow water outside the surf zone. Sound pressure levels with distance from rocky shorelines and pebble beaches have been investigated by Bardyshev et al. (1973) . However. a survey of the literature has not produced any reports on ambient measurements taken within the surf zone in sandy environments. This thesis presents the results of an underwater passive listening experiment in the surf zone during periods of energetic breaking: a simple experiment with results which are surprisingly simplified by the energetic environment in which it was carried out.

1.2 Thesis Motivation and Objectives

As a wave propagates toward the beach, the wave height increases as the water shoals and eventually an instability develops at the crest and the wave breaks. This region, where waves break due to decreasing mean water depth, is referred to as the surf zone.

Associated with the breaking is a large loss of wave energy, primarily in the form of turbulence. The turbulent motions generated by the breaking can, depending on the energy loss of the wave, reach the seabed and cause the suspension and transport of sediments (Fredsoe and Deigaard, 1992). Flows caused by the entrainment of air bubbles and their rise to the surface through buoyancy may help to carry sediments vertically upwards through the water column (although this has never been observed). Strong coastal currents in the surf zone are also driven by the momentum transferred during wave breaking and are an important mechanism in transporting sediment along the shoreline (Bowen, 1969). A description of sediment transport in the surf zone then depends upon the wave height, the amount of turbulence in the water and the currents induced, all of which are related to the energy dissipated in wave-breaking. A fraction of this energy loss is imparted to bubbles formed in the process, and subsequently radiated as sound through bubble oscillations. Therefore, the acoustic

signal generated by a breaking wave contains information relevant to wave energy dissipation, longshore current forcing, and nearshore sediment transport.

The experiment discussed in this thesis took place on a barred sandy beach as part of the Duck94 Nearshore Field Experiment. One problem envisaged with making ambient noise measurements in the surf zone, was that the noise of pounding surf on the shore might obscure the acoustic emissions of the individual breaking waves. There was also a concern that, because sound propagates farther in the spectral region of interest (between 100 Hz and 5 kHz), the range of listening would be so large as to make breaking events directly above indistinguishable in the midst of noise from distant breakers. The primary aim of the experiment was therefore to determine whether in fact useful information could be obtained from measurements of ambient noise in the surf zone.

This thesis is an exploration of some of the results from this experiment. It will be shown that, in a fully developed surf, ambient noise is mainly locally generated. The apparent screening of sound from distant sources, probably from the scattering and absorption effects of bubbles, allows the study of individual, local breaking events. This implies that ambient noise in the surf zone may be a useful measure of the frequency of breaking waves. The main objective is to provide a possible interpretation of the spectral record and use it to calculate the local breaking frequency.

1.3 Outline

The remainder of this thesis is organised as follows. Chapter 2 details the theory behind bubble-generated sound. In Chapter 3, the experiment, the instrumentation and data processing are described. The hydrophone's response to the underwater sound in the surf zone is presented in Chapter 4. Ambient noise is compared with wave height data in the surf zone and is used to calculate the change in local breaking frequency over the course of several days during the peak of a storm. The main conclusions to be drawn from these results are summarised in the final chapter.

Chapter 2

Mechanisms of Bubble Sound Generation

In the ocean, the mechanisms leading to bubble-generated acoustic emissions are numerous. Among them are bubble bursting, cavitation, shape oscillations, collisions between neighbouring bubbles, impact noise, volume pulsations of individual bubbles and collective oscillations of bubble clouds. There are also many phenomena in the upper layer of the ocean affecting bubble dynamics and, thus, bubble-generated sound: for example, surface tension, heat transport, orbital motion, turbulence, wave-breaking and gas dissolution. The complexity of this situation is lessened by considering the primary sound generating mechanisms for the simplified case of a spherical

bubble in an infinite liquid (Kolaini and Crum, 1994): first, the low amplitude breathing mode volume oscillations (also referred to as the natural resonance, Minnaert frequency, individual oscillation or zeroth order mode) of an individually entrained bubble and second, the coherent collective oscillation of the individual bubbles within a cloud. It is the intent of this chapter to outline these two dominant physical processes through which gas bubbles transmit sound to their fluid environment and to comment on secondary sound-producing mechanisms relevant to oceanic bubbles.

2.1 Individual Oscillations

A bubble in a fluid can be excited into resonance by an initial impulsive force, which Medwin and Beaky (1989) describe as shock excitation. Although there are many modes of oscillation which may result, only the resonant or zeroth order mode will be considered here. Small bubbles are approximately spherical due to surface tension effects and the equilibrium radius is determined by the balance of the liquid vapour pressure and air pressure inside the bubble, and of the surface tension and ambient pressure outside the bubble (Prosperetti, 1988b). A resonating spherical bubble in an infinite fluid will execute volume pulsations about its equilibrium volume and emit spherical pressure waves as a simple monopole source. The motion may be

approximated as simple harmonic since the dominant contributions of bubbles to ambient noise involve small amplitudes (Prosperetti. 1988b). In this system. because the mass of the bubble is negligible compared to the liquid medium. it is the displaced liquid which represents the inertia and the compressibility of the gas which produces the restoring force (Leighton. 1994).

2.1.1 The Resonance Frequency

The resonance frequency of a spherical gas bubble is estimated here summarising the method of Leighton (1994). We assume non-dissipative small amplitude motion of a polytropic gas bubble in an infinite. liquid. We also assume that the wavelength of sound emitted by the bubble is much larger than the bubble radius. so that the liquid is approximated as incompressible. This was first calculated by Minnaert in 1933. The method uses conservation of energy of the system and involves finding the maximum kinetic energy of the liquid at the bubble wall and equating it with the maximum internal energy of the gas in the bubble.

The bubble radius is given by the sum of the equilibrium radius and the time varying component which represents the oscillation of the bubble wall (Figure 2.1) at the resonance frequency ω_0.

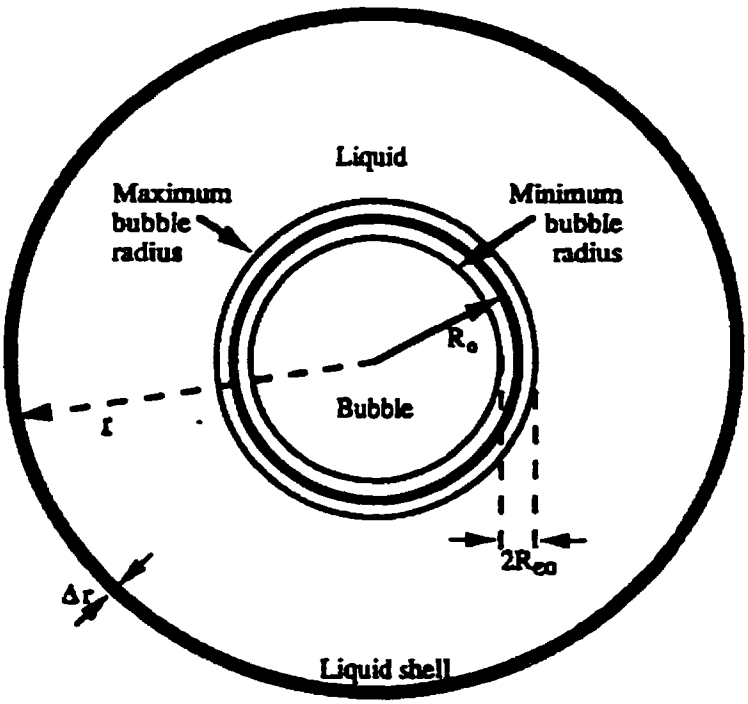

Figure 2.1: A bubble undergoing small amplitude linear oscillations. R_o is the bubble's equilibrium radius and R_{eo} is the amplitude of oscillation. The bubble is surrounded by spherical shells of liquid, of which one is shown with radius r and thickness Δr. Taken from Leighton, 1994.

$$R = R_o + R_e = R_o - R_{eo}e^{i\omega_0 t} \tag{2.1}$$

In order to calculate the kinetic energy of the liquid we integrate over the spherical volume of liquid from the bubble wall to infinity:

$$E_K = \frac{1}{2}\int_R^\infty 4\pi r^2 \rho dr\dot{r}^2 \tag{2.2}$$

where r is the radius of each infinitesimal liquid shell. $\dot{r} = \frac{\partial r}{\partial t}$, dr is the thickness and $4\pi r^2\rho dr$ is the mass.

As we have assumed the liquid to be incompressible we can equate the flow at the bubble surface to the flow through any spherical surface in the liquid centered at the bubbles origin. The mass of liquid, Q, passing through any of these spherical surfaces in time dt is $4\pi r^2\dot{r}\rho dt$. Equating Q to the flow at the bubble surface we can find a relation to substitute for $\dot{r}$ in the equation for E_K above:

$$4\pi r^2 \dot{r} \rho dt = 4\pi R^2 \dot{R} \rho dt \tag{2.3}$$

which gives

$$\frac{\dot{r}}{\dot{R}} = \frac{R^2}{r^2}. \tag{2.4}$$

Substituting Equation 2.4 into Equation 2.2 gives:

$$E_K = 2\pi\rho R^4 \dot{R}^2 \int_R^\infty \frac{dr}{r^2} = 2\pi\rho R^3 \dot{R}^2. \tag{2.5}$$

The maximum kinetic energy at the bubble wall occurs when it passes through the equilibrium radius. $R = R_o$. Substituting $R = R_o$ and $\dot{R}^2 = \omega_o^2 R_{eo}^2$ into Equation 2.5 we find the maximum kinetic energy in terms of the amplitude. R_{eo}. and frequency. ω_o. of oscillation.

$$E_K = 2\pi\rho R_o^3 \omega_o^2 R_{eo}^2. \tag{2.6}$$

The maximum potential energy of the bubble is equal to the amount of work done in compressing the bubble from it's equilibrium volume at R_o to it's minimum volume at $R_o - R_{eo}$. This is given by the integral of the differential pressure over the change in volume:

$$E_P = -\int_{R_o}^{R_o - R_{eo}} (p_g - p_o) 4\pi r^2 dr \tag{2.7}$$

where p_o equals the liquid pressure outside the bubble and p_g equals the instantaneous gas pressure inside the bubble. This pressure difference can be re-expressed using the polytropic relation PV^κ=constant where κ=1 for the isothermal case and γ for the adiabatic case.

$$p_o R_o^{3\kappa} = p_g (R_o + R_e)^{3\kappa} \tag{2.8}$$

Rearranging:

$$\frac{p_g}{p_o} = \frac{R_o}{(R_o + R_\epsilon)^{3\kappa}} = \left(1 + \frac{R_\epsilon}{R_o}\right)^{-3\kappa} \simeq 1 - 3\kappa\frac{R_\epsilon}{R_o} \tag{2.9}$$

$$\Rightarrow p_g - p_o = 3\kappa p_o \frac{R_\epsilon}{R_o} \tag{2.10}$$

and substituting into the equation for E_P leads to

$$E_P = \int_0^{R_{\epsilon o}} 3\kappa p_o \frac{R_\epsilon}{R_o} 4\pi R_o^2 dR_\epsilon = 6\pi\kappa p_o R_o R_{\epsilon o}^2 \tag{2.11}$$

for $r \sim R_o$. Equating the maximum kinetic energy (Equation 2.6) with the maximum potential energy (Equation 2.11) gives the Minnaert resonance frequency. $f = \omega_0/2\pi$. for a bubble of radius R:

$$f = \frac{1}{2\pi R_o}\sqrt{\frac{3\kappa p_o}{\rho}}. \tag{2.12}$$

For an air bubble in water we can assume adiabatic conditions so that $\kappa = \gamma$=1.4

and use ρ=1000 kg/m^3 and $p_o = 10^5(1+0.1z)$ N/m^2 where z is the depth of the bubble in metres. For air bubbles in water, Equation 2.12 then simplifies to

$$f = \frac{3.26}{R_o(cm)}(1 + 0.1z)^{1/2}. \tag{2.13}$$

As an example, consider a 1 mm radius bubble. At the surface f=3.26 kHz, at a depth z=2 m, f=3.57 kHz and at z=10 m, f=4.61 kHz. For near surface bubbles, Equation 2.12 can be simplified further to

$$f \simeq \frac{3.26}{R_o(cm)}. \tag{2.14}$$

2.1.2 Excitation Mechanisms

In recent years there has been much speculation about the mechanisms which induce the oscillations of individual bubbles. The initial suggestion by Wenz (1962) that the oscillations are excited by transient pressure fluctuations caused by turbulence to which bubbles are subjected as they rise to the surface has been ruled out by Crighton and Ffowcs Williams (1969). They note that the turbulent pressures are not likely to

remain coherent over length scales as large as the bubble radius and they are typically of a much lower frequency, from less than 1 Hz to perhaps 1 kHz, than the natural frequency of resonance of the bubble which is of the order of a few kilohertz (Kerman, 1984). Through experimental observations Pumphrey and Ffowcs Williams (1990) have concluded that the formation of bubbles at the surface through entrainment and shearing is the most likely time for bubbles to be excited into resonance. Therefore it is left to formulate possible excitation mechanisms associated with the entrainment process. Various theories have been put forward by Longuet-Higgins (1990a) for bubbles entrained through water-drop impact, and extended for bubbles entrained by breaking waves by Pumphrey and Ffowcs Williams (1990). Three of the theories they present are discussed below (note this discussion only considers excitation of the spherically symmetric resonance mode).

Excitation through the hydrostatic and Laplace (surface tension) pressures supposes that at the instant of closure of the liquid around the bubble, the gas inside the bubble will be subject to the additional pressures from the liquid surrounding the bubble and due to surface tension or the Laplace pressure (Hollett and Heitmeyer, 1991; Leighton, 1994; Pumphrey and Ffowcs Williams, 1990). This will cause compression of the gas inside and subsequent oscillations about an equilibrium volume. Consider the gas in the bubble immediately before the moment when the liquid en-

capsulates the gas. There will still be some orifice connecting the bubble with the atmosphere so that the gas will be at atmospheric pressure, p_{atm} (Figure 2.2).

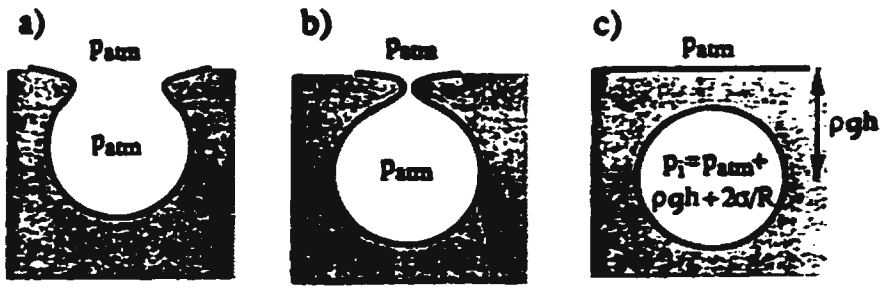

Figure 2.2: The gas pressures in the formation of a bubble. In a) and b) the air initially entrapped by the liquid is at atmopheric pressure. At the moment of closure the bubble is subject to the additional hydrostatic and Laplace pressures, c). Taken from Leighton, 1994.

When the liquid closes the gas is instantaneously subject to the same atmospheric pressure plus the hydrostatic pressure, ρgh (h = depth) plus the Laplace pressure, $2\sigma/a_o$ (a_o = equilibrium radius). The bubble then collapses through the equilibrium radius, a_o, where the internal pressure of the gas $p = p_{atm} + p_\sigma + \rho gh$, to a minimum radius where $p = p_{atm} + 2(p_s + \rho gh)$ due to the inertia of the liquid. Assuming no damping it will expand to its original maximum radius at formation and continue oscillating sinusoidally about a_o.

Longuet-Higgins (1990a) has suggested that surface waves on a bubble may couple to the resonance mode and initiate volume pulsations. When bubbles are formed they are generally non-spherical in shape and the distortions can be in the

form of large amplitude surface waves. This coupling is especially likely to occur if the resonance frequency is twice that of the surface mode. For example. Figure 2.3 shows a spherical bubble and the same bubble distorted into a shape with the same volume but a different surface area. The natural tendancy of a non-spherical bubble is to minimize the surface energy by enclosing the gas in as small a surface area as possible. Assuming that the distorted bubble then returns to a spherical shape the extra energy that went into distorting the bubble may be transferred to volumetric oscillations.

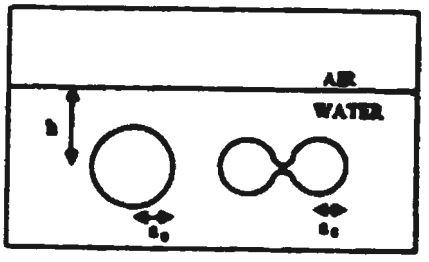

Figure 2.3: A bubble may be excited into volume oscillations from a coupling between surface waves on the bubble and the bubbles resonance mode. From Pumphrey and Ffowcs Williams, 1990.

At the instant of enclosure of the gas in the bubble it is also probable that there is a radial flow around the bubble (Figure 2.4). This situation would evidently lead to an initial volume change and therefore to excitement of the resonant mode. Based on theoretical studies of these mechanisms, it has not been possible to conclude that

in any given circumstance there is one dominant mechanism for excitation. However, there does appear to be a strong dependence on depth and on bubble radius.

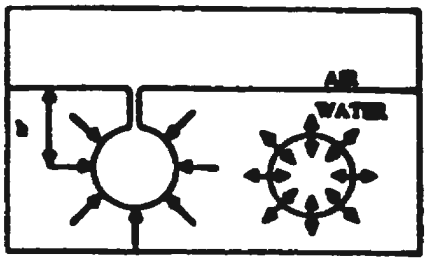

Figure 2.4: Sketch showing radial flow around a bubble as it is entrained. From Pumphrey and Ffowcs Williams, 1990.

2.2 Collective Oscillations of a Bubble Cloud

Bubbles created by breaking waves in the ocean are likely to occur in high enough concentrations that interactions between neighbouring bubbles in a bubble cloud may become important. The cloud, excited by the emissions of individual bubbles, may act as a system of coupled oscillators radiating normal modes at a much lower frequency than the resonant frequency of the individual constituent bubbles. The effect of these bubble clouds may be even more important in the ocean than in fresh water as bubbles formed in salt water tend to have smaller mean radii, occur at higher concentrations, and rise more slowly to the surface. It is believed that this low frequency sound

radiated by bubble clouds may be the most significant contribution to the broad maximum around 300-500 Hz which occurs in measured oceanic ambient noise spectra levels. The observed low frequency peak would require a bubble with a radius of the order of one centimetre which are unlikely to exist in sufficient numbers to account for the observed intensities. This section will examine the hypothetical formation of bubble clouds in the ocean following Monahan and Lu (1990), and describe a simple method of estimating the lowest order resonant mode of a bubble cloud (Lu et al., 1990).

2.2.1 Ocean Bubble Characteristics

As mentioned before, the entrainment of air into the ocean takes place mainly through wave breaking. The subsequent behaviour of the bubbles depends on factors such as their size, local currents, and surfactants. One curious characteristic of ocean bubbles, summarized by Leighton (1994), is the persistence of foam on the sea surface. Foam lies on top of the surface and is probably made of larger bubbles that have risen to the surface and which can then remain for 10 to 60 seconds. Generally foam is not acoustically active because an individual bubble in contact with its nearest neighbours does not couple well with its environment. Bubbles which lie beneath the surface are quite

likely to emit sound. At wind speeds greater than or equal to approximately 7 m/s there is a continuous bubbly layer just below the surface (Leighton. 1994). Bubbles which are transported by turbulence or Langmuir circulation to greater depths may be grouped together in clouds which may oscillate collectively.

Monahan and Lu (1990) describe in detail the various stages of bubble plume formation. The first stage is the formation. by an active whitecap or an aerated spilling wave crest. of a concentrated α plume. with void fractions as much as 8%. The individual bubbles in this plume are thought to act as incoherent monopole sources of sound at kHz frequencies. The lifetime of an α plume is generally less than 1 second and it will decay into a plume of type β unless it is periodically regenerated by parent spilling breakers. A β plume is associated with a mature whitecap or hazy foam patch and may have a lifetime on the order of 10 seconds. Void fraction estimates range from 0.01-0.02 % to 0.1-0.2 % (Leighton. 1994). The plume as a whole may be a coherent source of low frequency sound through collective oscillations of the plume. The final stage is the most abundant type of plume. denoted γ. which has a lifetime on the order of hundreds of seconds. void fractions of 10^{-4} to 10^{-6} %. and remains acoustically detectable long after the spilling wave has gone.

2.2.2 Collective Oscillations

When a wave breaks an appreciable amount of initial energy is imparted to bubbles formed in the process. Some of this energy is radiated as sound and, while the oscillations of individual bubbles are a strong source of high frequency sound, there are not enough bubbles of large enough size to account for the sound levels observed at low frequencies. Prosperetti (1988a and 1988b) suggested that the source of these low frequencies may be the coupling of individual bubbles in a cloud which oscillates at normal modes at low frequencies.

An alternative argument is described by Lu et al. (1990). The bubbly mixture within the cloud can be seen as another medium with the speed of sound generally much smaller than in pure liquid. If the walls of the cloud were rigid, then it would have a set of normal modes dependent upon the cloud size. Because the bubble walls are not rigid in reality, the acoustic energy, which would otherwise be trapped within the cloud, leaks out into the surrounding liquid and is subsequently detected as sound. However, the normal modes can be estimated by considering a cloud with rigid walls of linear dimension L and containing N bubbles. The sound speed in the bubbly mixture (Carey and Browning, 1988) is given by

$$c_m = \left(\frac{p_o}{\rho \beta (1 - \beta)} \right)^{1/2} \tag{2.15}$$

where p_o= undisturbed pressure, and β=void fraction. Assuming β to be small we can neglect the $(1-\beta)$ term and using $L = \lambda/2$ for the lowest order mode and $\omega = kc$ we get

$$\omega_m = k c_m = \frac{\pi}{L} \left(\frac{p_o}{\rho \beta} \right)^{1/2}. \tag{2.16}$$

If the cloud is approximated as a sphere of radius L with N bubbles of radius R, then the void fraction $\beta = N(R/L)^3$. To compare the cloud oscillation with the individual bubble oscillations we find the ratio of ω_m to the Minnaert frequency. $\omega = 2\pi f$ calculated in 2.1.1.

$$\frac{\omega_m}{\omega} = \frac{\pi R}{L} \left(\frac{1}{3\kappa\beta} \right)^{1/2} = \frac{\pi}{\sqrt{3\kappa}} \frac{1}{(\beta^{1/6} N^{1/3})} \tag{2.17}$$

Since β is to such a low power, the ratio is not strongly dependent on β and

therefore the frequency of the cloud's normal modes will be approximately proportional to the inverse of the cube of the number of bubbles in the cloud. For example, if the number of bubbles N=1000, then the first order normal mode will be about an order of magnitude smaller than the frequency of the individual bubbles.

Chapter 3

The Experiment

3.1 Duck94 and the Experiment Site

The Duck94 Nearshore Field Experiment took place in October 1994 at the US Army Corps of Engineers Waterways Experiment Station Field Research Facility (FRF) located in Duck, North Carolina (Figure 3.1). Facing the open Atlantic, the FRF has in the past hosted a series of collaborative experiments geared towards understanding nearshore dynamics. Duck94 was a continuation of this series and involved the efforts of 11 universities (2 Canadian), 3 private U.S. companies and 6 U.S. federal agencies. The research objectives of the experiment focussed on the dynamics of sediment transport and morphology and on nearshore hydrodynamics.

The FRF is located on a long straight sandy coast which is unbroken for 100 km. With the exception of several fishing piers and the FRF's 561 m long pier, there are no major coastal structures or littoral barriers along this stretch. Mean sand grain size is between 0.38 and 0.52 mm, decreasing offshore. Offshore incident wave forcing conditions at the FRF are monitored continuously with a pressure sensor array at 8 m depth. Meteorological data are also collected daily. The FRF operates a 10 m high Coastal Research Amphibious Buggy (CRAB) which is used to conduct surveys of the bathymetry in the nearshore and which can operate in wave heights up to 1.8 m. Bathymetric profiles are collected on a monthly basis except during experiments when a minigrid of the area around the instrumentation is surveyed daily. The CRAB is also useful in the deployment of instruments in the surf zone.

During the month of October, a common feature is the occurrence of a sand bar on the order of 100 m from the shoreline. Significant migration of the bar is also typical. The longshore current is variable in direction. However, during periods of intense storms generated by Nor'easters, the longshore current is southward. Experiments are generally carried out on the north side of the pier so the effect of the pier is reduced during storms.

Duck94 was scheduled for October, and a typical storm developed, after the instruments were deployed, on October 10th. It lasted for 8-9 days and gradually

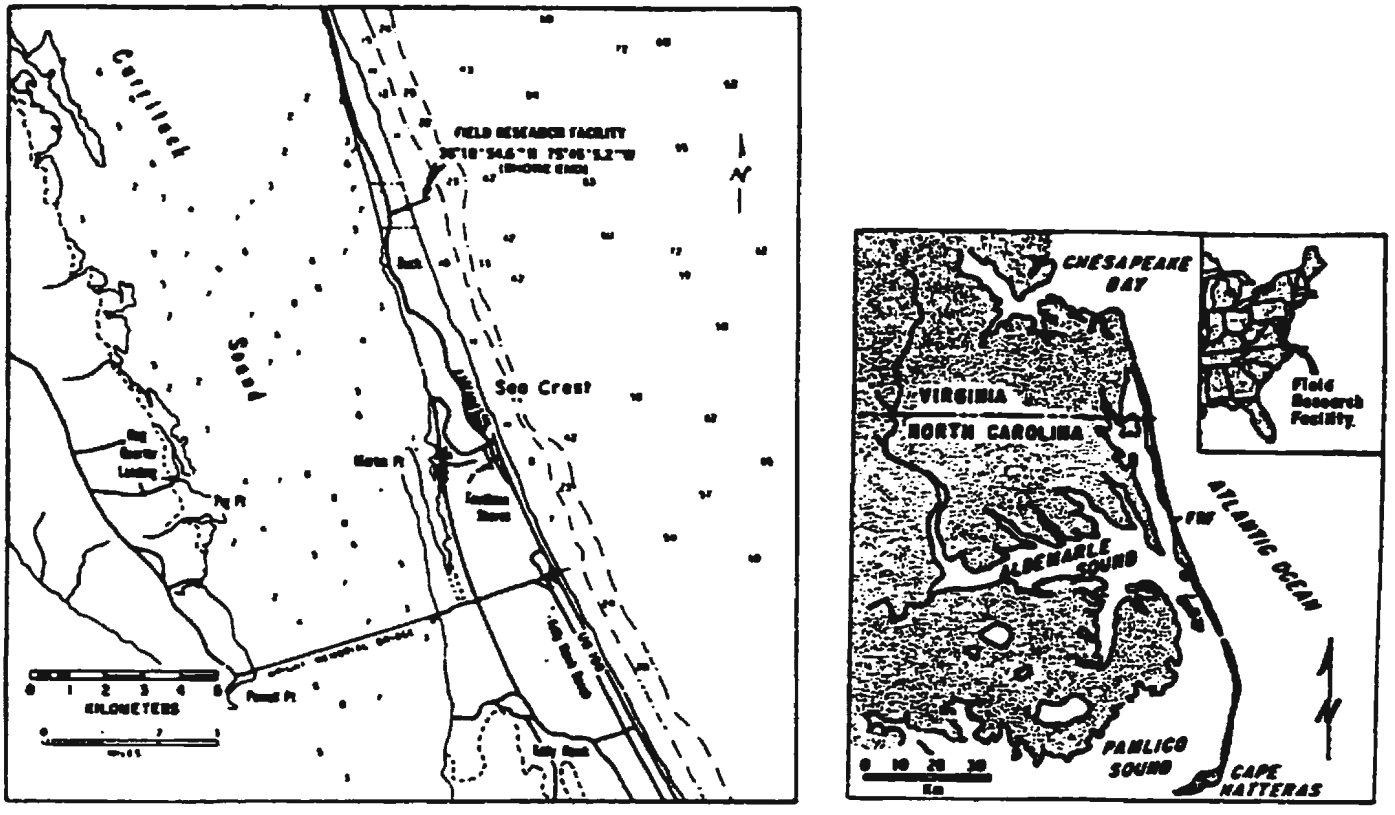

Figure 3.1: Location of the US Army Field Research Facility.

subsided, creating a full range of wave types, bedforms and active sediment transport.

3.2 Instrumentation

Ambient noise was measured with an ITC-6050 C omnidirectional broadband hydrophone clamped to a 5 cm diameter steel post which was embedded 5 m into the seabed. The bandwidth of the hydrophone was 70 kHz. Figure 3.2 shows the location of the hydrophone at approximately 85 m from the shoreline on the shoreward side of the sand bar, about 1 m above bottom, in a water depth of 2 m. Waves were generally of plunging type on the sand bar and on the shoreline. In times of high surf, breakers on the bar, having subsided into spilling breakers, would pass over, and be detected by, the hydrophone.

Wave height data were obtained from a pressure sensor and an upward-looking Simrad-Mesotech pencil beam sonar operating at 2.25 MHz; both mounted on a frame located about 20 m shoreward of the hydrophone on the same cross-shore profile line. A video camera set up onshore provided continuous monitoring of the ocean surface in the vicinity of the hydrophone.

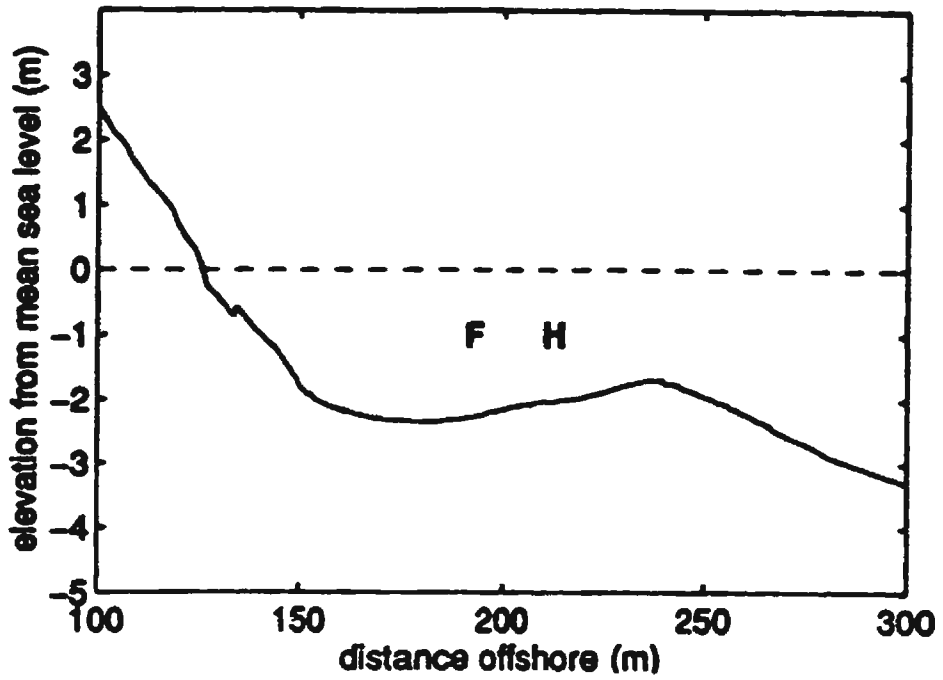

Figure 3.2: Profile of the sandy beach showing the location of the instruments. H represents the hydrophone which was located about 1 m below the surface on the shoreward side of the sand bar. The location of the frame holding the pressure sensor and the pencil beam sonar is marked by F.

3.3 Data Acquisition and Processing

Underwater ambient noise and the sea surface video were recorded simultaneously on high-grade VHS video tapes. Data were collected during the day from October 10 throughout the storm until the 21st. The recorded hydrophone signal was first electronically high and low-pass filtered respectively at 120 Hz and 10 kHz, and then 2048 point sets were digitally acquired at 20 kHz, averaging adjacent samples and multiplying each set by a Hammimg window. The resolution of the spectra is about 20 Hz. FFT's (1024 point) were computed using a digital signal processor (DSP)

which was triggered at a rate of 8 Hz. The FFT's were then normalised and averaged in pairs to obtain spectra at a rate of 4 Hz with a Nyquist frequency of 5 kHz. Data were stored in files containing 2280 sets where each set was composed of a time stamp, the unprocessed, 'raw', voltage response of the hydrophone corresponding to the first trigger in the averaged FFT pair, the averaged FFT's, and the standard deviation of the FFT's before averaging. Each file represents 570 seconds of data and has a stored size of 9.4 Mbytes. Synchronization of the hydrophone data and the video was accomplished through a time code reader which recorded the time imbedded in the video image. Individual frames were converted to digital format for computer analysis using the Matlab data analysis package.

The pressure was recorded continuously at 10 Hz in files 30 minutes in length. Wave statistics were calculated (Long, 1994) for each half hour record to provide information with which to compare the hydrophone data. The mean sea level for a half hour period was calculated as the mean of the pressure record while the significant wave height was calculated by multiplying the standard deviation of the pressure record by four (Horikawa, 1988). The wave period was determined by smoothing the power spectrum and selecting the peak.

Upward looking pencil beam data were collected every 30 minutes for 190 seconds. Sound was transmitted at a rate of about 18 Hz and the recorded sound

averaged over 3 transmissions. Backscattered sound was sampled at a rate of 250 kHz then averaged over 3 samples to obtain a range resolution of approximately 9 mm. Pressure and pencil beam sonar data are not available after the morning of October 15th because of damage to the frame.

Chapter 4

Results

4.1 Introduction

Ambient noise measurements were made in the frequency range 120 Hz to 5 kHz during the course of the storm which started on October 10th. The storm lasted nine days with peak wave periods initially close to 7 seconds and offshore wave heights approximately between 1.5 and 2.5 metres. This peak storm period was characterized by persistent breaking on the bar and between the bar and the beach, and widespread bubbles and foam in the surf zone. After the 14th of October, peak wave periods increased to 10 to 12 seconds and the offshore wave height peaked at 4.05 metres on the 15th and then steadily decreased to about 1.3 metres on the 20th. Peak wave

periods remained in the same interval until the 18th when they rose to 13 to 15 seconds and remained there until the end of the experiment.

In periods of low energy surf, when the wind speed was low and there was little spray in the air, the overwater video provided a very clear comparison between wave breaking events and the corresponding acoustic signal received by the hydrophone. Results from low energy conditions allow a better identification of the source mechanisms of the underwater sound and are consequently the initial topic of discussion in this chapter. During energetic surf conditions, before 15 October, the sound detected by the hydrophone appeared to be localised to the region around the hydrophone. Wave height data, from the pressure sensor and pencil beam sonar, were available before the 15th so that the hydrophone response to individual breaking waves could be compared with wave heights and the occurrence of bubble clouds evident in the sonar images. Ambient noise spectral series acquired in heavy surf also provide a means of estimating local wave breaking frequency. The results presented in this chapter are divided into those acquired during low and high energy surf.

4.2 Low Energy Conditions

4.2.1 Breaking Events

Two series of video frames from October 17 during the waning stages of the storm are shown in Figures 4.1-4.2 and 4.3-4.4. During this period the surf was still fully developed, yet the quantity of foam on the surface of the water was not so great as to compromise the clarity of the video image reproduced on paper. Figures 4.1-4.2 and 4.3-4.4 each show a series of 8 video frames, at one second intervals, of breaking events in the surf zone. The corresponding ambient noise spectra with 20 degrees of freedom, averaged over one second, are displayed alongside the video frames. In the video images, the hydrophone location, indicated by the black and white 'X', is about 5 m seaward of a marker post. The time is shown at the bottom of the images in hours, minutes, seconds and 1/30 seconds (EST). In the spectral plots, the amplitude units on the y axis are arbitrary. Absolute sound pressure levels are not necessary as the analysis of the spectra is only concerned with relative sound level changes with time.

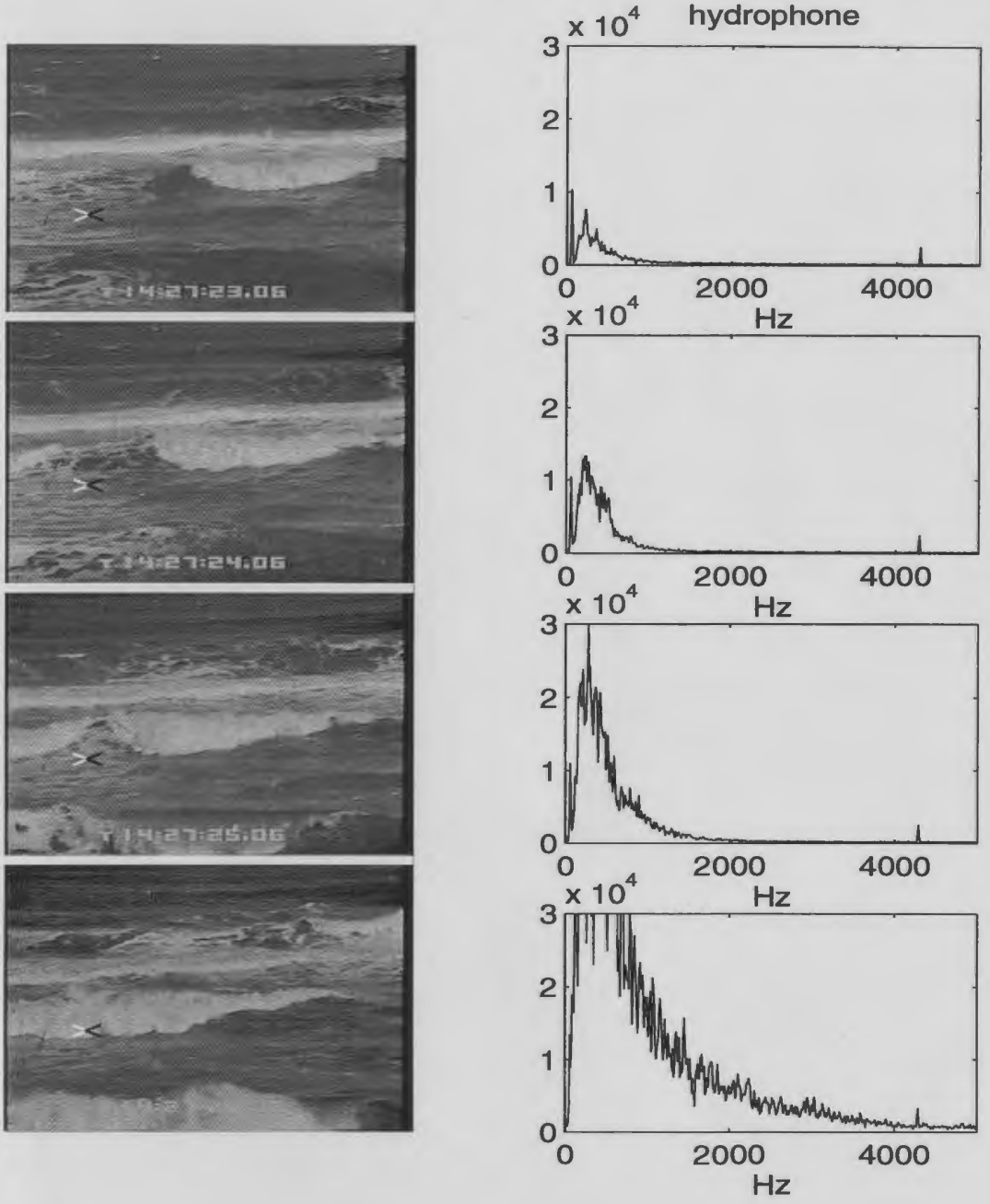

Figure 4.1: The first half of a series of 8 video frames at 1 s intervals during a breaking event starting at 14:27:23 on October 17. The hydrophone location is marked by the black and white 'X'. The corresponding ambient noise spectra averaged over 1 s intervals are plotted on the right. This series continues in Figure 4.2.

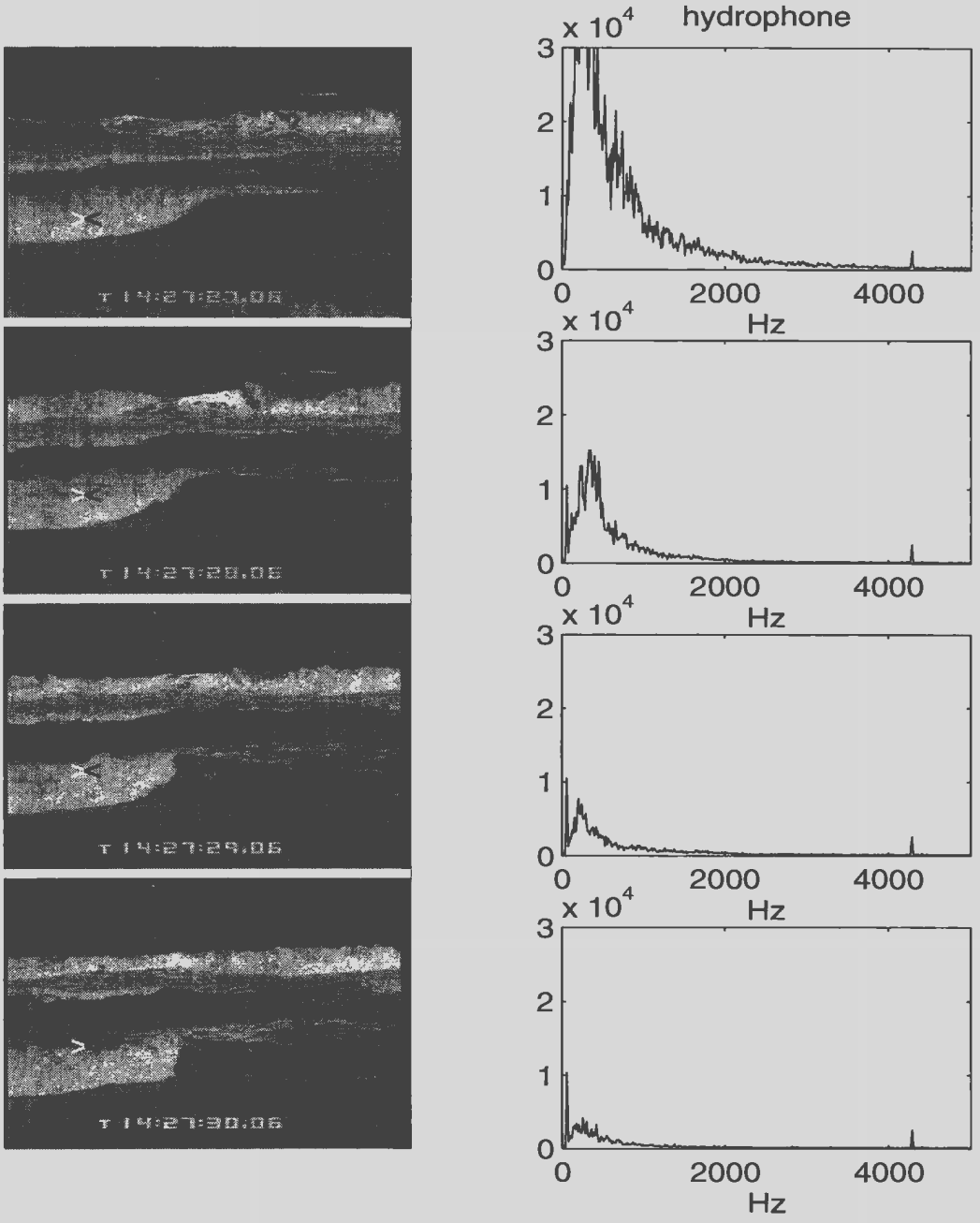

Figure 4.2: The second half of a series of 8 video frames at 1 s intervals during a breaking event starting at 14:27:23 on October 17. The hydrophone location is marked by the black and white 'X'. The corresponding ambient noise spectra averaged over 1 s intervals are plotted on the right. This series is continued from Figure 4.1.

The spectral series in Figure 4.1-4.2 is typical of the hydrophone response during the passage of an energetic spilling breaker. Sharp peaks occurring in all spectra at 60 Hz and above 4 kHz are due to electrical noise. The wave depicted in this series had previously broken at 2 points along the wave crest and these 2 break points converged just above the hydrophone at 14:27:26 in Figure 4.1. In this event background noise levels were observed 2 to 3 seconds before the wave reached the hydrophone. Once the breaker had passed the hydrophone there was a rapid decrease in noise to background levels (to be discussed later in this section).

The following breaking event in Figure 4.3-4.4 is not quite so energetic. In the first 3 seconds shown the breaker can be heard approaching the hydrophone and there is an apparent gradual increase in intensities below 1 kHz. Once the wave reaches the hydrophone at 14:25:24, intensities increase over the entire spectrum up to 5 kHz. This is followed by a dramatic drop in intensities throughout the full spectrum until background noise levels are reached at 14:25:28. The small spectral peak occurring around 4 kHz at 14:25:24 is associated with splashing sounds heard on the tape. Considering the hydrophone's response to the approach of the breaker in Figure 4.3-4.4, the series in 4.1-4.2 indicates a smaller listening radius in the first few seconds. The noise levels from both breakers are reduced to background levels within 2 to 3 seconds after the passage of the waves over the hydrophone.

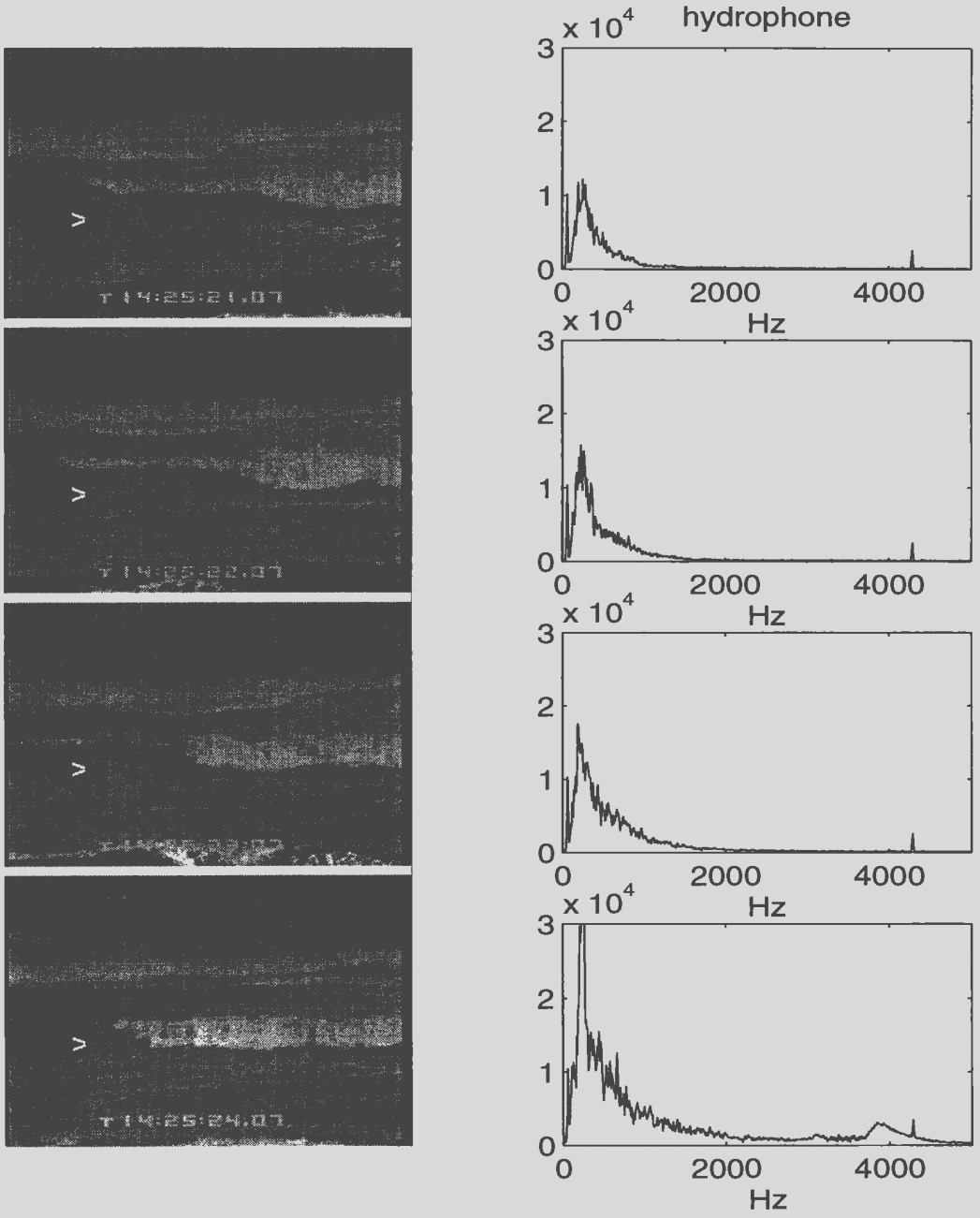

Figure 4.3: The first half of a series of 8 video frames at 1 s intervals during a breaking event starting at 14:25:21 on October 17. The hydrophone location is marked by the black and white 'X'. The corresponding ambient noise spectra averaged over 1 s intervals are plotted on the right. This series continues in Figure 4.4.

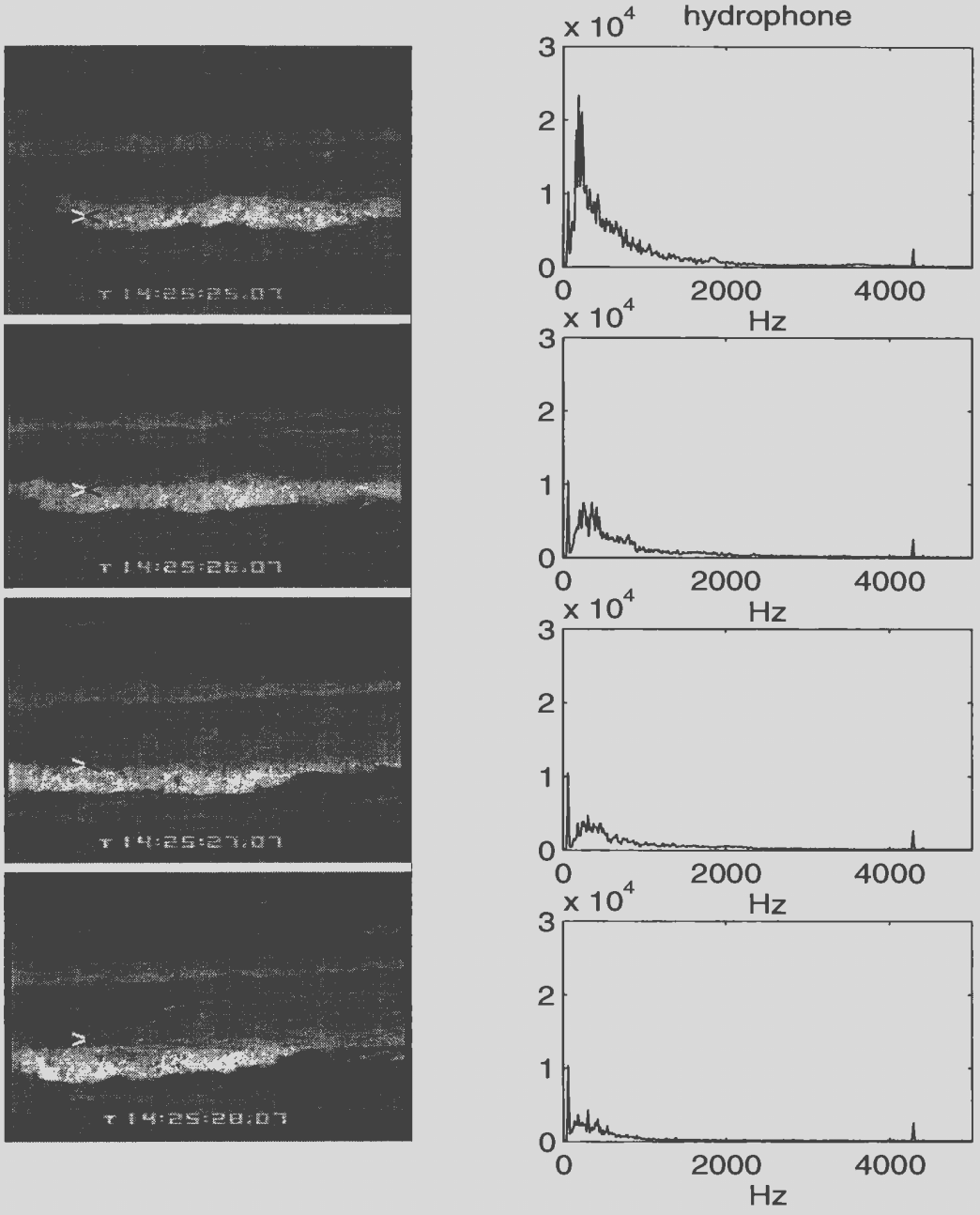

Figure 4.4: The second half of a series of 8 video frames at 1 s intervals during a breaking event starting at 14:25:21 on October 17. The hydrophone location is marked by the black and white 'X'. The corresponding ambient noise spectra averaged over 1 s intervals are plotted on the right. This series is continued from Figure 4.3.

In both figures the sound appears to be due to the breaking process. The foam in the wake of the breaker does not appear to be very acoustically active, possibly for reasons mentioned in section 2.2.1

Figures 4.5 and 4.6 are spectral time series from the same period from which the previous two breaking events in Figures 4.1-4.2 and 4.3-4.4 (respectively denoted Breaker A and Breaker B) were taken. Both figures are segments of a data file 570 seconds in length. The time axes in Figures 4.5 and 4.6 represent the time in seconds from the start of the data file. Darker shades represent higher sound intensities. Breaker A in Figures 4.1-4.2 appears in Figure 4.5 at approximately 176 seconds: Breaker B (in Figures 4.3-4.4) occurs at 54 seconds in Figure 4.6.

The video showed that other breaking events above the hydrophone occur in Figure 4.5 at 168, 198, 208 and 238 seconds. The events at 198 and 208 are gently spilling breakers while those at 168, 176 and 238 are more energetic with larger bubble plumes or rollers (Fredsoe and Deigaard, 1992) on the forward face of the wave. A small spill just to the side of the hydrophone occurs at 218 seconds. The only breaking event directly above the hydrophone in Figure 4.6 is Breaker B at 54 seconds. A small spill nearby is seen preceding Breaker B at 45 seconds. The events which occurred above the hydrophone are marked by strong sound intensities predominantly below 500 Hz and increases in sound levels above 1 kHz of shorter duration. The more

energetic the spill the higher the intensities at all frequencies. Non-breaking events, which will be discussed later, are evident at 187 and 231 seconds in Figure 4.5 and at 35, 61 and 91 seconds in Figure 4.6.

From Figures 4.5 and 4.6 the breaking waves above the hydrophone appear quite distinctly amongst the spectral time series above background noise levels. The sound profile during an energetic breaking event appears to be characterized by an initial increase in intensities at low frequencies which then moves to high frequencies and is followed by a rapid decrease to background levels. Breakers appear to be detected only when they are in the immediate vicinity of the hydrophone. This limited detection distance, particularly after the passage of a breaker, is suggestive of a screening effect of bubbles on sound from distant sources, as discussed below. Breaker B occurred in a relatively calm period, no other breaking events above the hydrophone are evident in the recorded video for Figure 4.6. On the other hand, Breaker A occurred amidst a series of breaking waves, in particular, ten seconds after a fairly energetic breaker. Because the quantity of air entrained into the water is most likely greater in Figure 4.5 than 4.6, the proposed screening of sound by bubbles would delay the detection by the hydrophone of the approach of Breaker A (at 175 s in Figure 4.5). The air entrained through breaking is naturally concentrated near the upper layer of the ocean. As noted by Farmer and Vagle (1988a), the stratification in density in this air-water

mixture tends to refract sound up into the low sound speed bubbly layer near the surface where it is more effectively dissipated by scattering and absorption by bubbles. The localisation of sound is thus enhanced by this acoustic energy trapping near the surface. Restricted detection distances in the frequency range of interest are also readily apparent from observations of the video and hydrophone signal during many instances where large plunging breakers occur on the bar about 40 metres beyond the hydrophone but are not detected acoustically.

The effective listening radius of the hydrophone may be estimated from the phase speed of the wave. As an example, this radius is estimated for Breaker A (Figure 4.1-4.2 and 175 s in Figure 4.5). Assuming shallow-water wave theory, the phase speed, c, of the wave is given by $c = \sqrt{gh}$ (Gill, 1982) where g is the gravitational constant and h is the water depth. Near the hydrophone, the water depth, h, is approximately 2 m which gives a phase speed of about 4.5 m/s. The return of the ambient sound to background levels following the breaking wave takes place in 2 to 3 seconds. This implies an effective listening radius of 9 to 14 m.

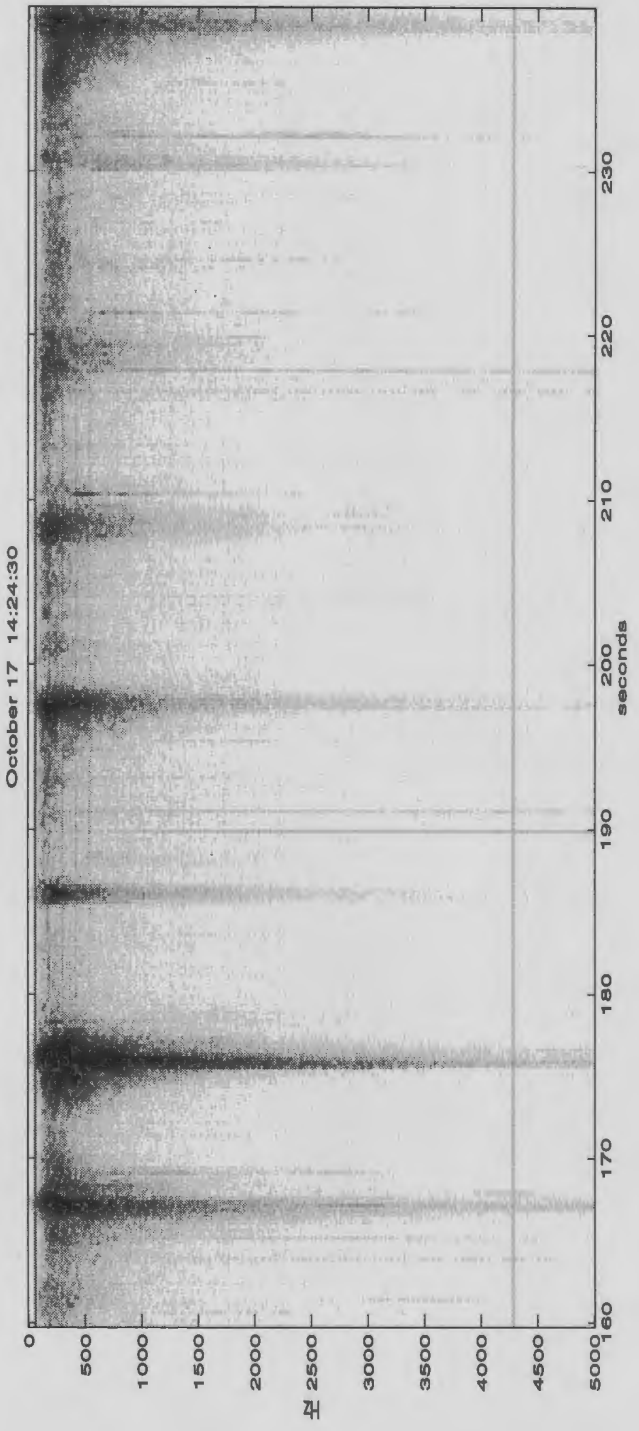

Figure 4.5: Spectral time series from October 17. Time is elapsed time in seconds from 14:24:30 start. The event at 14:27:26 in Figure 4.1 (Breaker A) occurs at 176 s.

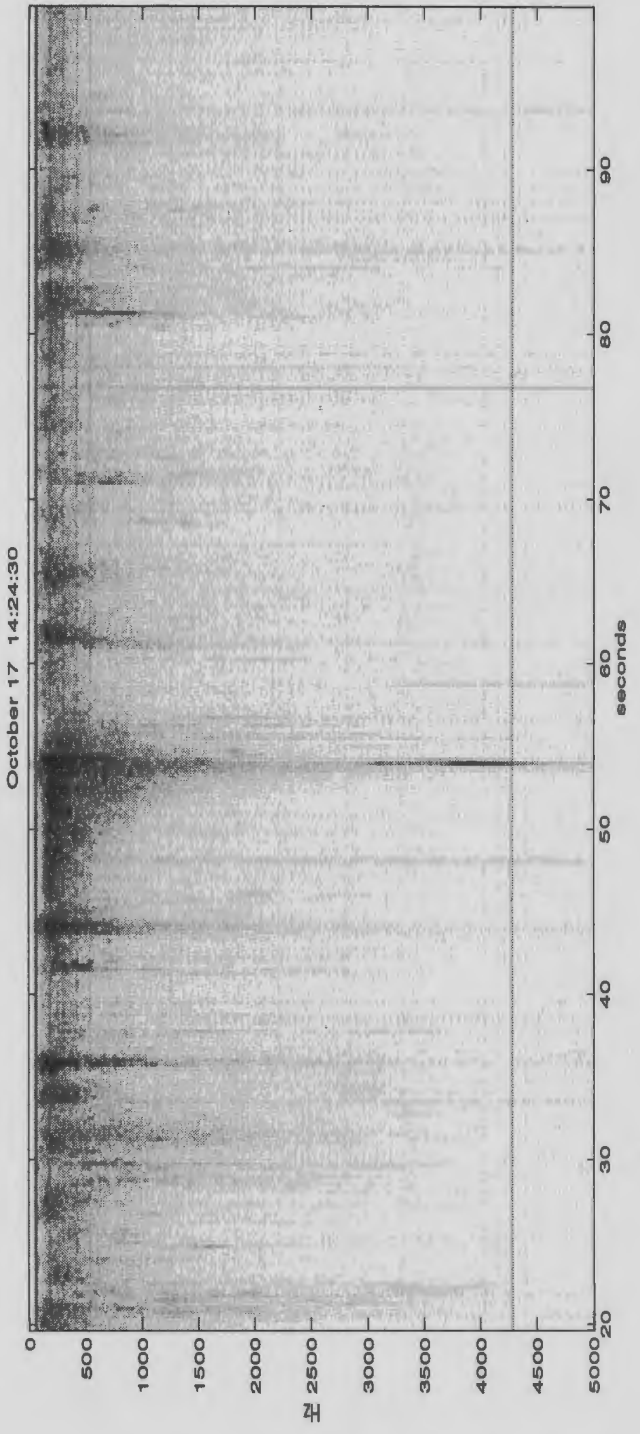

Figure 4.6: Spectral time series from October 17. Time is elapsed time in seconds from 14:24:30 start. The event at 14:25:24 in Figure 4.3 (Breaker B) occurs at 54 s.

4.2.2 Individual Bubble Oscillations

A relatively less energetic interval, from the same data file from which Figures 4.5 and 4.6 were taken, is shown in Figure 4.7. Splashing sounds were heard at 244 and 253 seconds and appear to be connected to the high intensity narrow frequency band points occurring between about 200 Hz and 1 kHz at these times. These sounds are suggested to be the volume pulsations of individual bubbles close to the hydrophone. This possibility was investigated by looking at some of the hydrophone voltage time series (the raw data) at times when these narrow frequency band points occur. For example, the 1100 Hz pulse at 287 seconds in Figure 4.7 is shown as a time series in Figure 4.8. This frequency is equivalent to the resonance frequency of a 3 mm radius bubble. Approximate sound pressure levels can be calculated by multiplying the hydrophone response in mV by 0.034 Pa/mV, so a 100 mV signal gives a sound pressure level of 3.4 Pa. Sound pressure levels, of about 1 Pa, from individual bubble oscillations at a distance on the order of a metre, were recorded by Updegraff and Anderson (1991) and Medwin and Beaky (1989).

The voltage data in Figure 4.9 correspond to 291 seconds in Figure 4.7 and show 2 distinct frequencies around 800 and 450 Hz which correspond respectively to bubble radii of 4 and 7 mm. Finally, Figure 4.10, which corresponds to the pulse

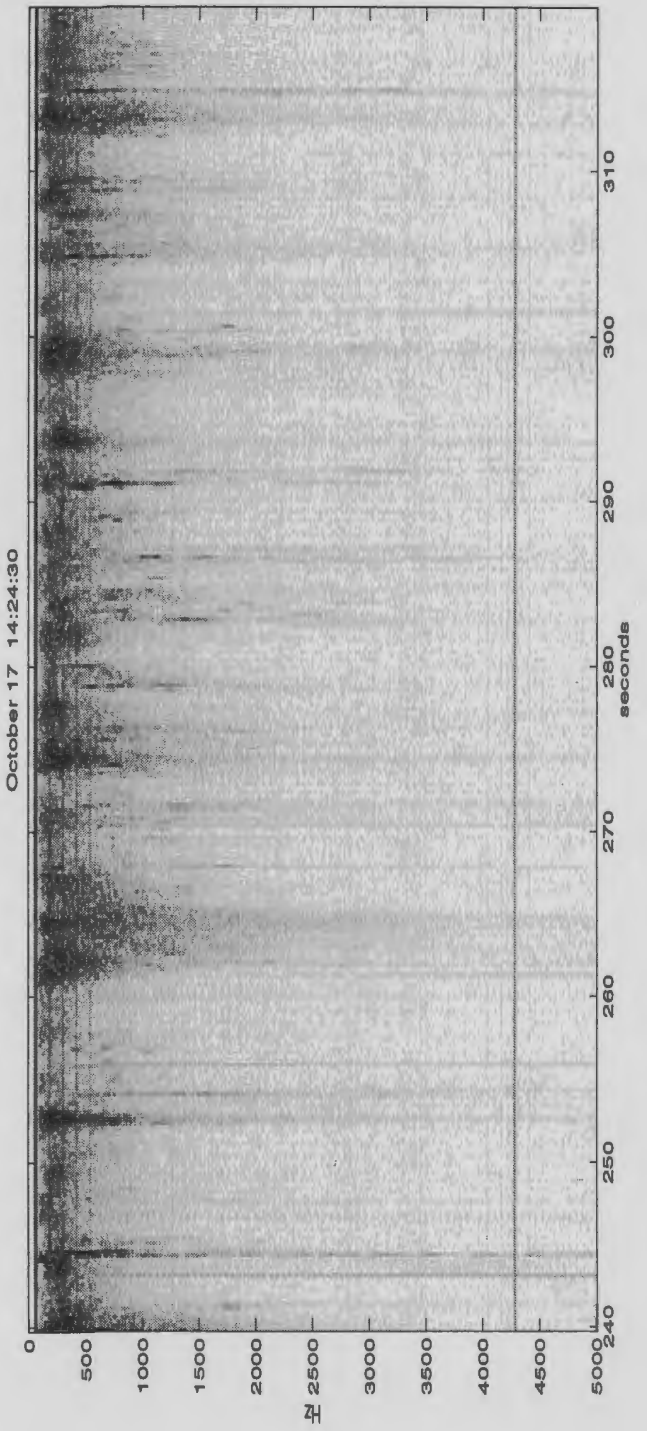

Figure 4.7: Spectral time series from October 17. Time is elapsed time in seconds from 14:24:30 start.

at 210 seconds in Figure 4.5. depicts a lower frequency resonance of about 400 Hz and a duration on the order of ten milliseconds. These figures are typical of the signatures from individual bubble oscillations and are similar to the results obtained by Medwin and Beaky (1989) from laboratory spilling breakers and by Updegraff and Anderson (1991) from gently spilling waves recorded 1 metre below the ocean surface. Both recorded sound from spills which was composed of distinct resonant bubble oscillations with decay times of several milliseconds. Individual bubble signatures have been classified by shape and described by Medwin and Beaky (1989).

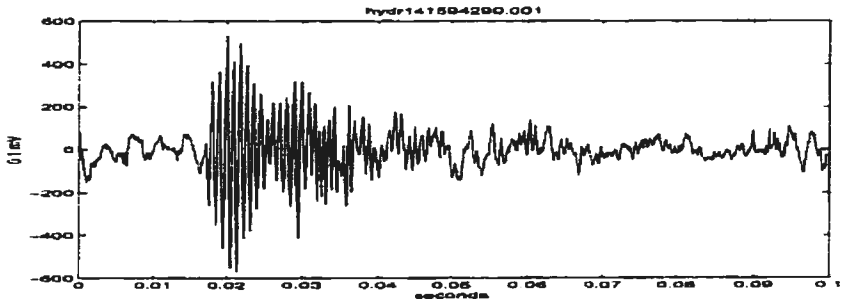

Figure 4.8: An individual bubble resonance from 287 seconds in the October 17 spectral time series (figure 4.7).

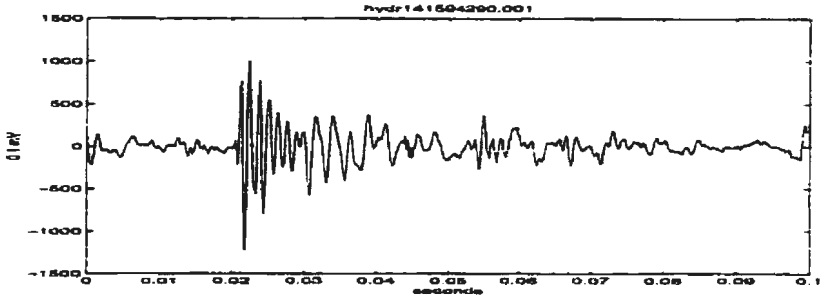

Figure 4.9: An individual bubble resonance from 291 seconds in the October 17 spectral time series (figure 4.7).

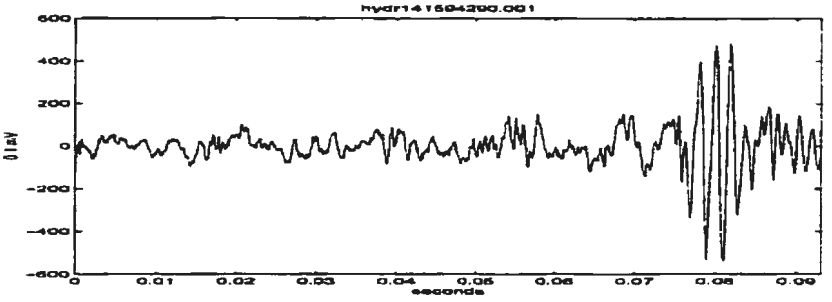

Figure 4.10: An individual bubble resonance from 210 seconds in the October 17 spectral time series (figure 4.6).

4.2.3 Other Sounds

In Figure 4.7 the sounds detected by the hydrophone appear at times to be generated some distance from the hydrophone so that identification of the sources of sound are not as readily determined as in Figures 4.5 and 4.6. For example, in Figure 4.7 at 293 seconds, a wave crashing on the shore, some 70 m away, is detected. Other distinguishable sounds were produced by a very light spill occurring around 263 seconds above the hydrophone and a small spill near the hydrophone at 312

seconds.

One problem that was encountered in identifying waves breaking above the hydrophone was a combination of broad and narrow band signals produced during the passage of a high but non-breaking wave over the hydrophone. Figure 4.11 displays the spectral time series of a 150 second interval recorded in the morning of October 19 at the end of the storm. This interval was marked by long-period waves occasionally breaking on the bar. Examples of the signals produced by non-breaking events appear in Figure 4.11 at 39, 62, 72, 85, 122, and 135 seconds. Breaking waves above the hydrophone occurred at 2, 15, 28, 48, and 102 seconds in Figure 4.11. The breaker at 28 seconds was not breaking as it approached the hydrophone but plunged directly on top thus accounting for the lack of signal on approach. The breaking events in Figure 4.11 are readily distinguished from the non-breaking events by the temporal breadth (approximately one wave period) of the signal generated by the breakers, particularly at frequencies below 500 Hz. However, it is also probable that the type of signal caused by non-breaking events is also present during the passage of breaking waves. Non-breaking events were also apparent in the spectra presented earlier, i.e in Figure 4.5 at 187 and 231 seconds and in Figure 4.6 at 35, 61 and 91 seconds.

The source of this sound from non-breaking events is a matter of some speculation. These sounds appear to occur particularly with the passage of high waves

and high velocity flow. The narrow frequency band peaks around 200 Hz (seen in the spectral series in Figure 4.11 as small black curves below 500 Hz) are possibly caused by flow past the instrumentation. Eddy shedding from a circular cylinder creates an oscillation in velocity of the flow behind the cylinder at a frequency given by the Strouhal number, $S=fd/U\simeq 0.21$, where f is the frequency of vortex shedding, d is the diameter of the cylinder and U is the flow velocity beyond the boundary layer (Kundu, 1990). From shallow-water wave theory the horizontal water particle velocity in shallow water is given by $u=ca/H$, where c is the wave phase speed, a is the wave amplitude, and H is water depth. Flow velocities caused by a wave may then be around 2 m/s. For a 200 Hz eddy shedding frequency, the diameter of the cylinder would then be 2 mm, which is much smaller than the diameters of cables and instrument mounting hardware. Consequently, this sound does not appear to be due to eddy shedding from anything known. However, it is possible that eddy shedding from a sharp edge, such as the clamps on the hydrophone, would create sound at a discrete frequency which varies with flow velocity.

The broad band sound is dominant below 500 Hz but can extend as far as kilohertz frequencies, particularly for larger waves. Possibilities may be the sound caused by shifting sand or sand laden flow past the hydrophone.

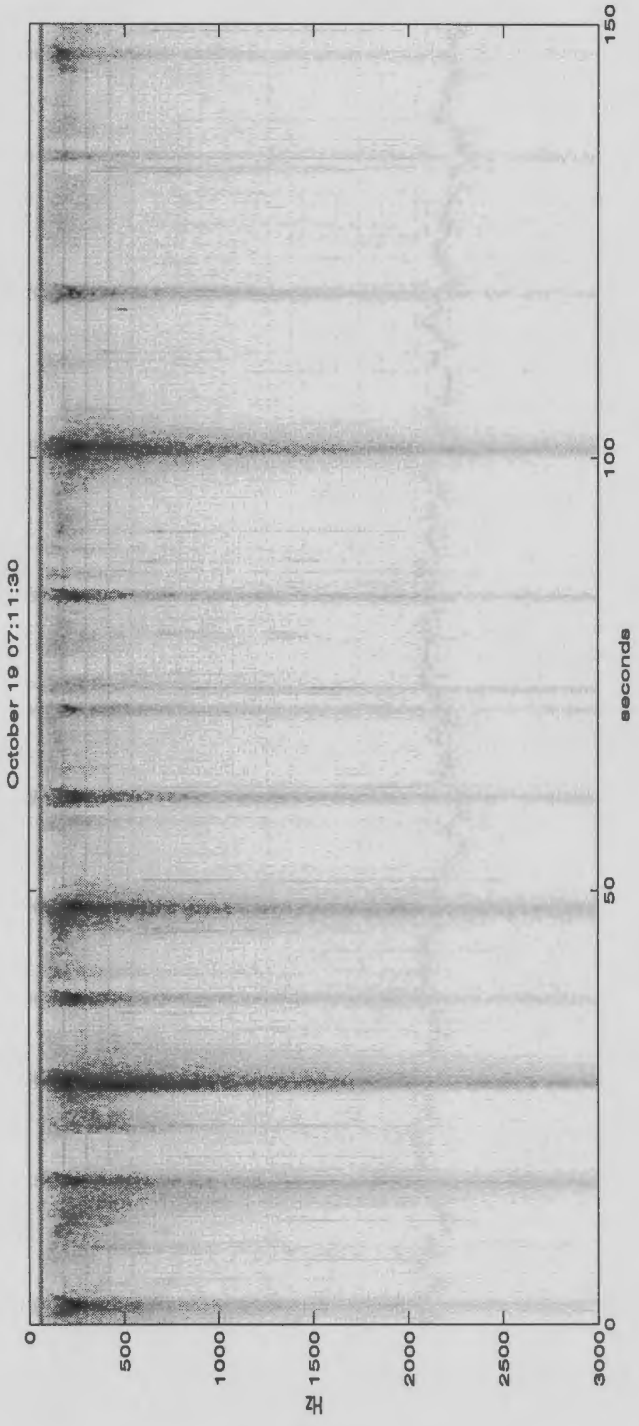

Figure 4.11: Spectral time series from October 19. Time is elapsed time in seconds from 07:11:30 start.

4.3 High Energy Conditions

4.3.1 Comparison of the Spectra with Wave Heights

The following set of Figures. 4.12 to 4.19. display various intervals in the ambient spectra along with the wave height data represented by the pressure change and the acoustic backscatter from the upward-looking pencil beam sonar. These intervals. from October 13th to 15th. were chosen because the wave energy was high at these times and because the video image was clear. The y-axis in the pressure and pencil beam plots represents the distance from the sensors so that both plots depict an upside-down image of the sea surface. In the pencil beam images. the darker patches beneath the waves are due to backscatter from bubble clouds. There is good correlation between the pressure signal and the sea surface elevation detected by the sonar. Observable differences in wave amplitude and peakiness between the pressure and sonar images of the sea surface are due to the greater resolution of the sonar to small amplitude fluctuations. These differences are attributable to the fact that small amplitude changes, translated as pressure changes are not transmitted to the depth of the pressure sensor which is approximately 1 metre deep. In the pencil beam images of Figures 4.13. 4.17 and 4.18, bubbles are present in high enough concentrations that the sound emitted by the pencil beam is completely scattered or absorbed and the

ocean surface is obscured for portions of the record.

To account for wave propagation over the distance of 20 m separating the hydrophone and sonar locations, the pressure and pencil beam data have been appropriately lagged, assuming shallow water wave theory, 4 seconds behind the hydrophone data so that comparisons may be made more directly. Intensities in the spectral images have been normalised by the maximum intensity in each interval and plotted on the same grayscale. The dark horizontal lines occurring in the spectra are again due to electrical noise.

As discussed below, Figures 4.12 to 4.19 demonstrate that:

1. The ambient noise spectra are dominated by discrete events of increased intensities. In the data presented, increases are initially evident at low frequencies and progress to higher frequencies, followed by decay first at high then progressively lower frequencies. The events are often asymmetric, with slower growth and more rapid decay.

2. High waves do not necessarily produce much noise. This indicates that the flow noise, discussed in section 4.2.3, is not a problem in these data.

3. Noise events at the hydrophone 'peak' during the passage of wave crests.

4. A sequence of quite substantial waves can sometimes produce no noise events, even from the initial break on the bar or from the shore break.

5. The occurrence of bubble plumes at the sonar location is not obviously correlated

with noise events at the hydrophone location.

6. Points 2. to 5. above are consistent with the association between noise events and local breaking inferred from the overwater video.

The ambient noise spectra shown in Figures 4.12 to 4.19 are dominated by discrete events associated with breaking waves. These events appear to be characterized by an initial increase in intensities at low frequencies, then progressively to higher frequencies, followed by decay first at high frequencies, then at progressively lower frequencies. The distinctness of these events is particularly well displayed in Figures 4.12 and 4.13 from October 13 where wave breaking was more energetic than in the later figures. The last 3 events in Figure 4.12 and most in Figure 4.13 are accompanied by periods of comparative silence, with background noise levels, before and after the passage of the breaker. The asymmetrical shape of most of the spectral events, similar to Breaker B, at 54 seconds in Figure 4.6, is also notable. There appears to be an initial increase in intensities at low frequencies which gradually moves to higher frequencies and then quickly to intensity increases over most of the spectrum. The decay of sound levels at all frequencies is generally more rapid than the rise. This shape is especially apparent, for example, in Figure 4.15 at 31, 41, and 62 seconds, Figure 4.16 at 61 seconds, and Figure 4.19 at 10, 30, and 40 seconds. Event durations are typically one wave period (7-10 seconds).

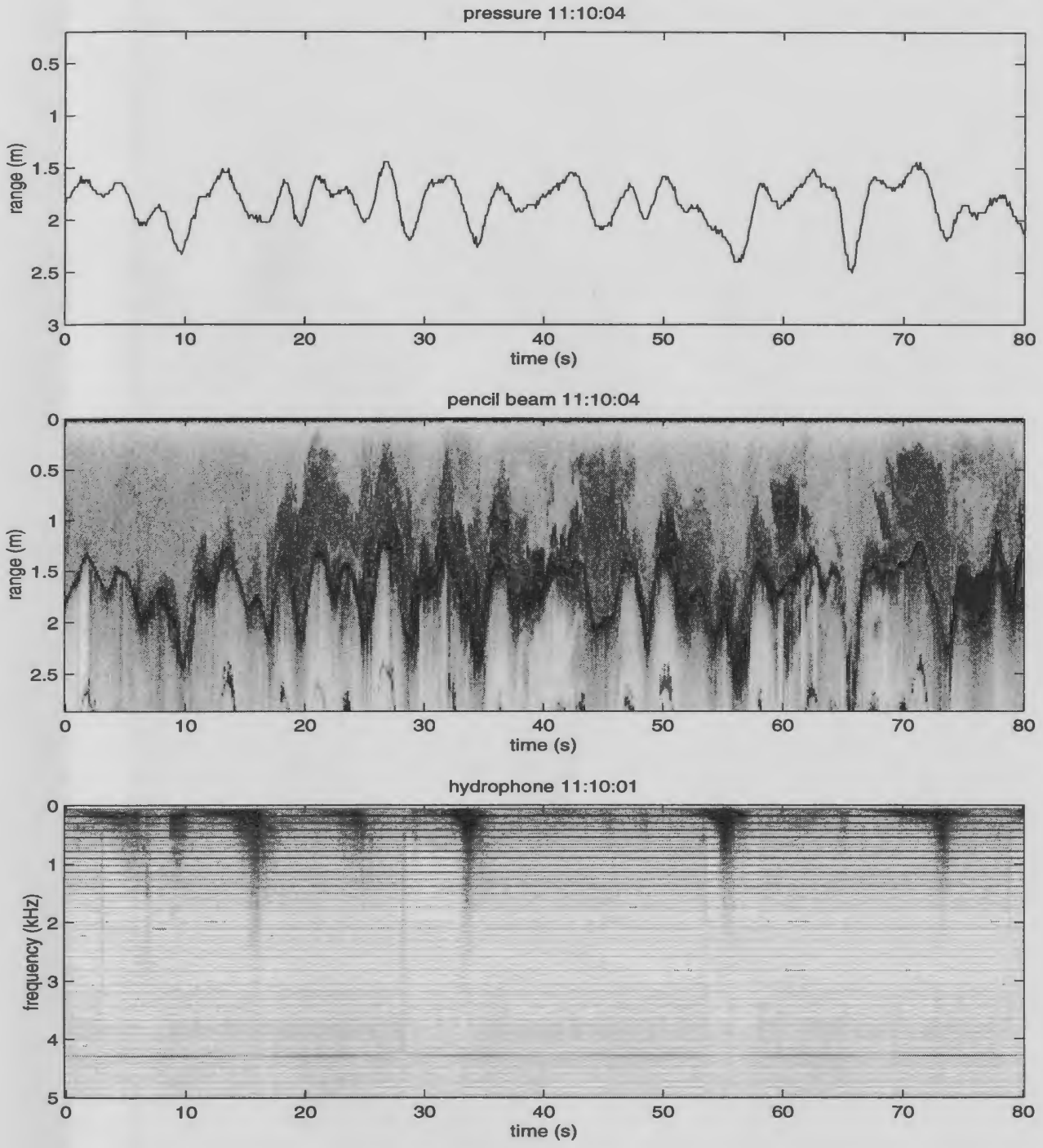

Figure 4.12: Time series taken from data from October 13 showing the pressure (top), the acoustic backscatter from the pencil beam (middle) and the spectra recorded from the hydrophone (bottom).

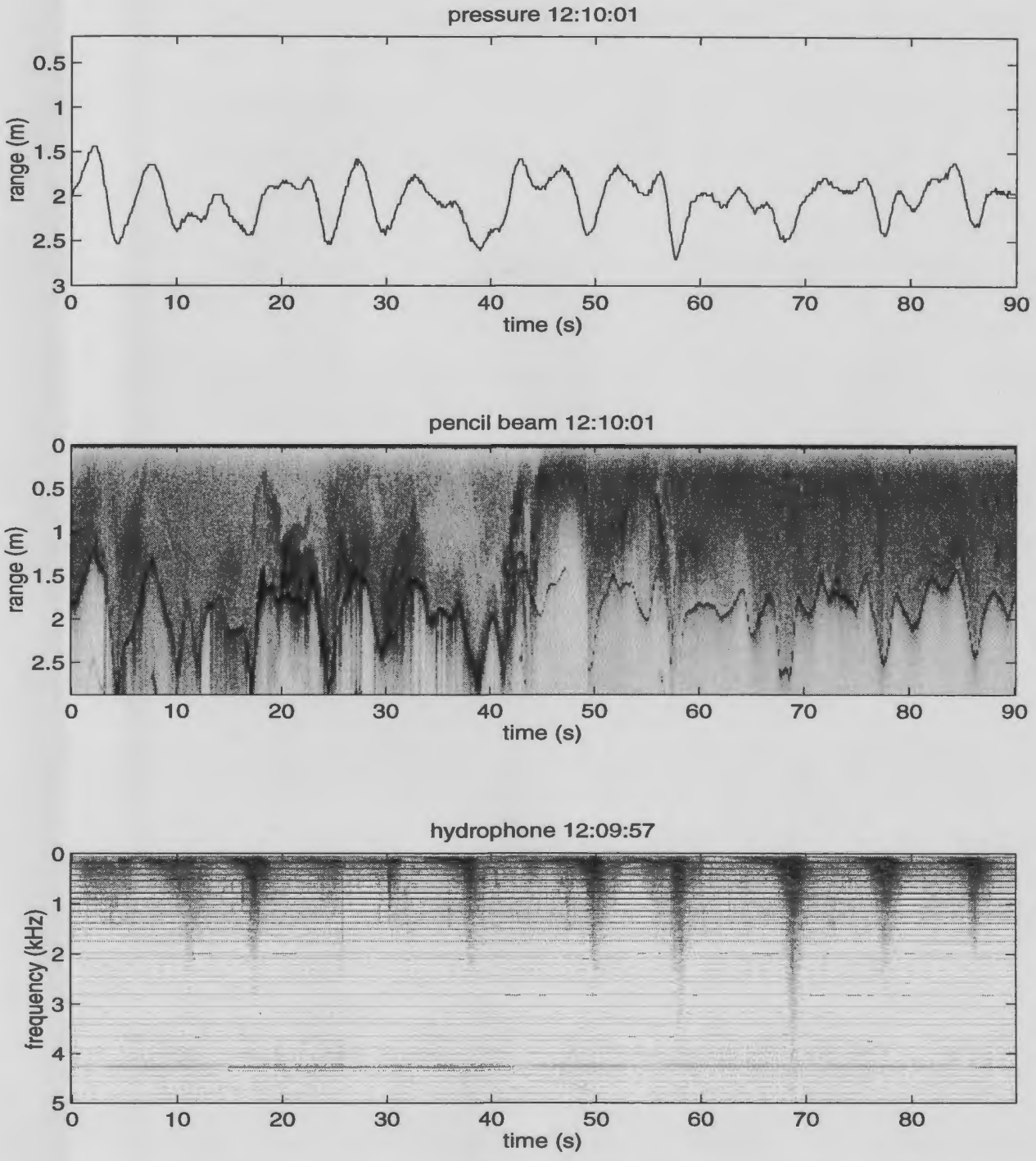

Figure 4.13: Time series taken from data from October 13 showing the pressure (top), the acoustic backscatter from the pencil beam (middle) and the spectra recorded from the hydrophone (bottom).

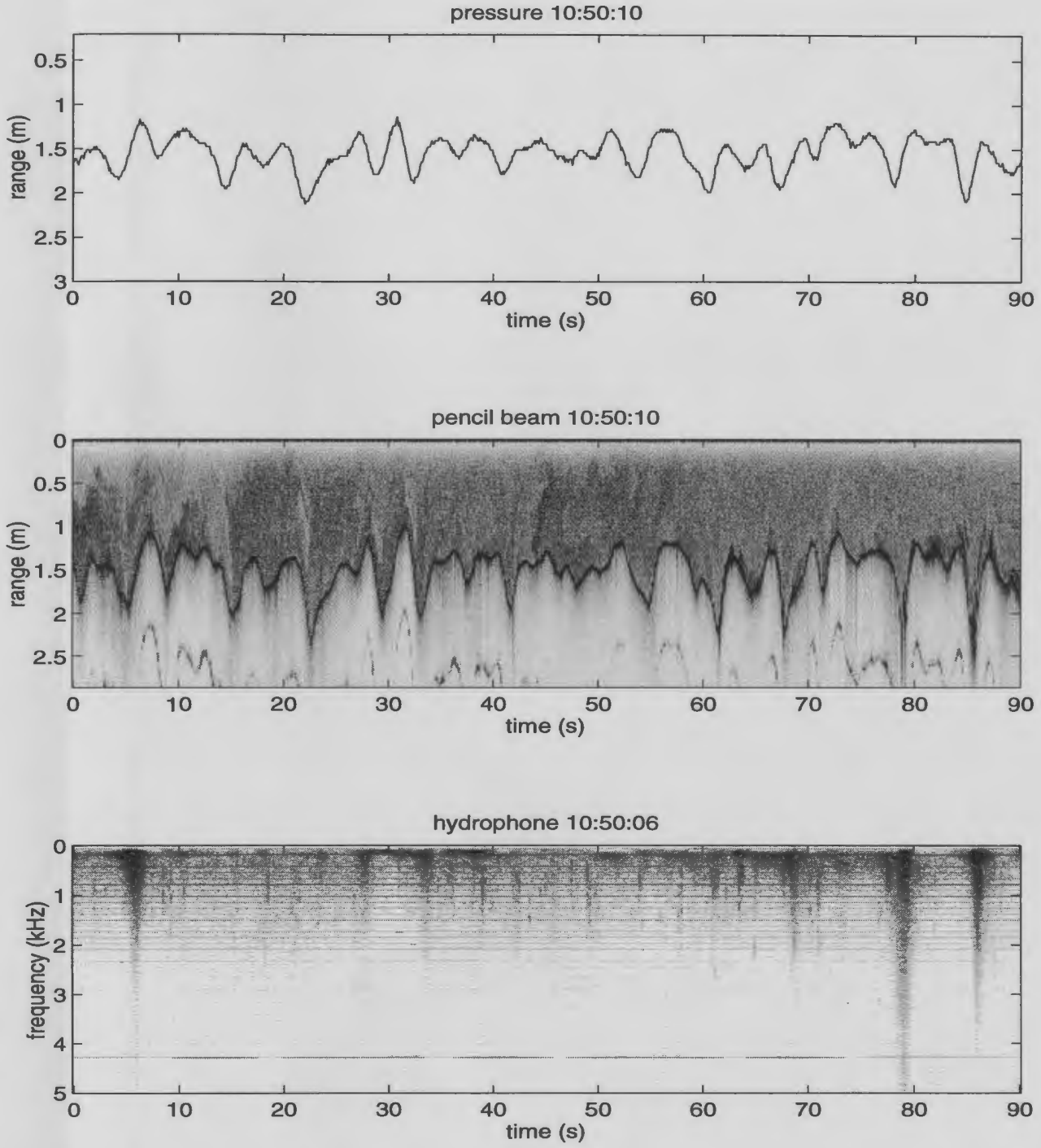

Figure 4.14: Time series taken from data from October 14 showing the pressure (top), the acoustic backscatter from the pencil beam (middle) and the spectra recorded from the hydrophone (bottom).

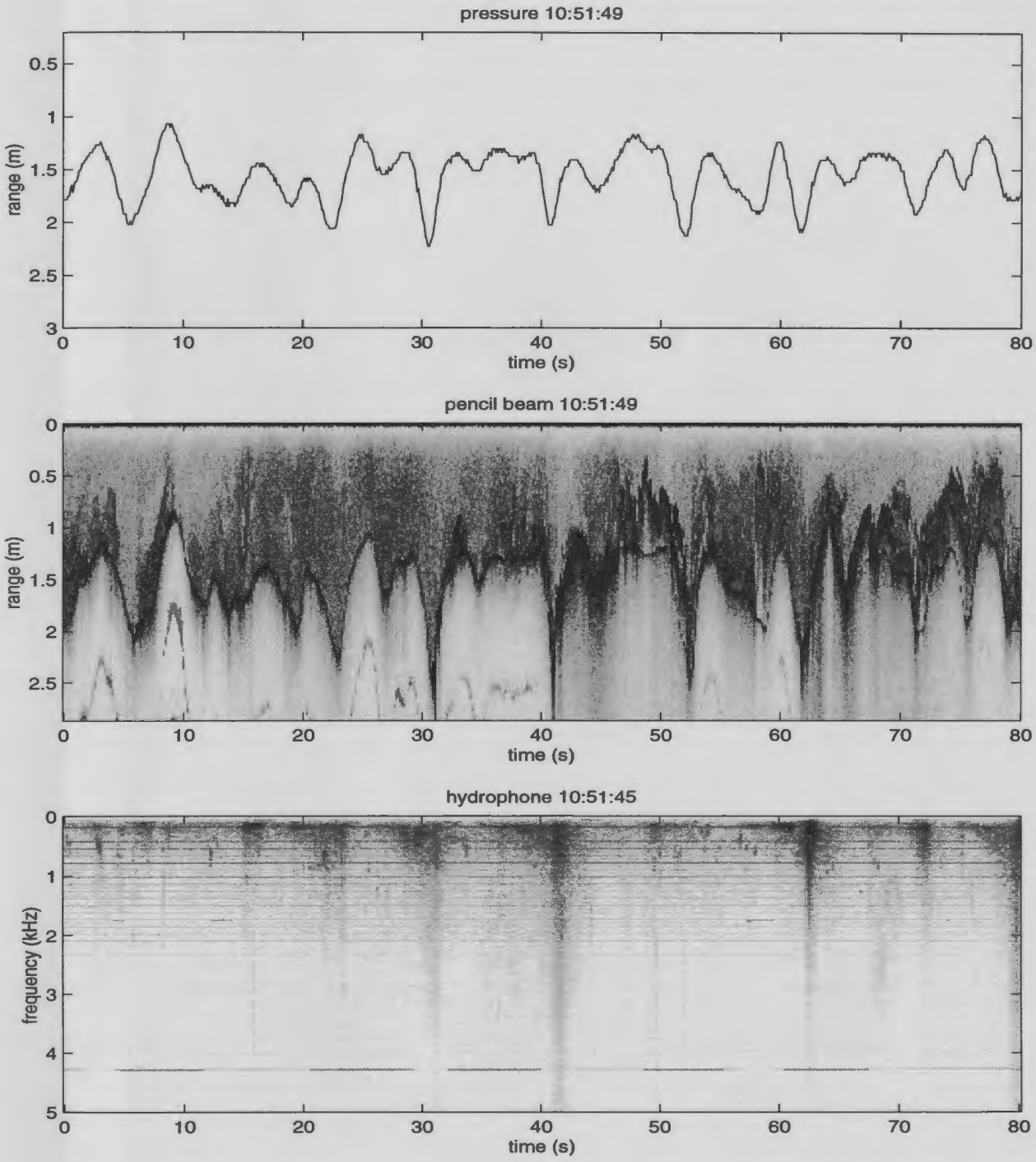

Figure 4.15: Time series taken from data from October 14 showing the pressure (top), the acoustic backscatter from the pencil beam (middle) and the spectra recorded from the hydrophone (bottom).

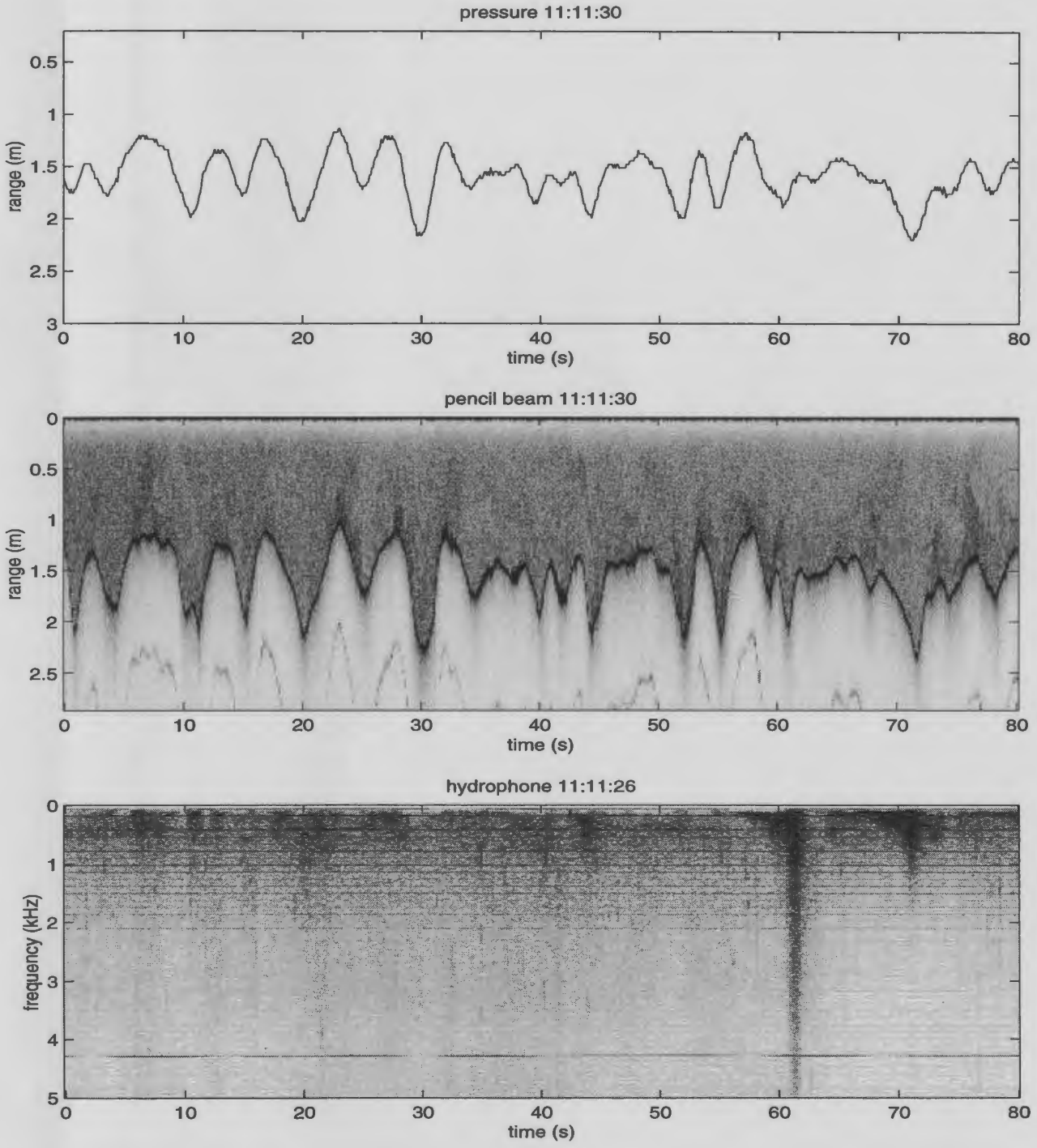

Figure 4.16: Time series taken from data from October 14 showing the pressure (top), the acoustic backscatter from the pencil beam (middle) and the spectra recorded from the hydrophone (bottom).

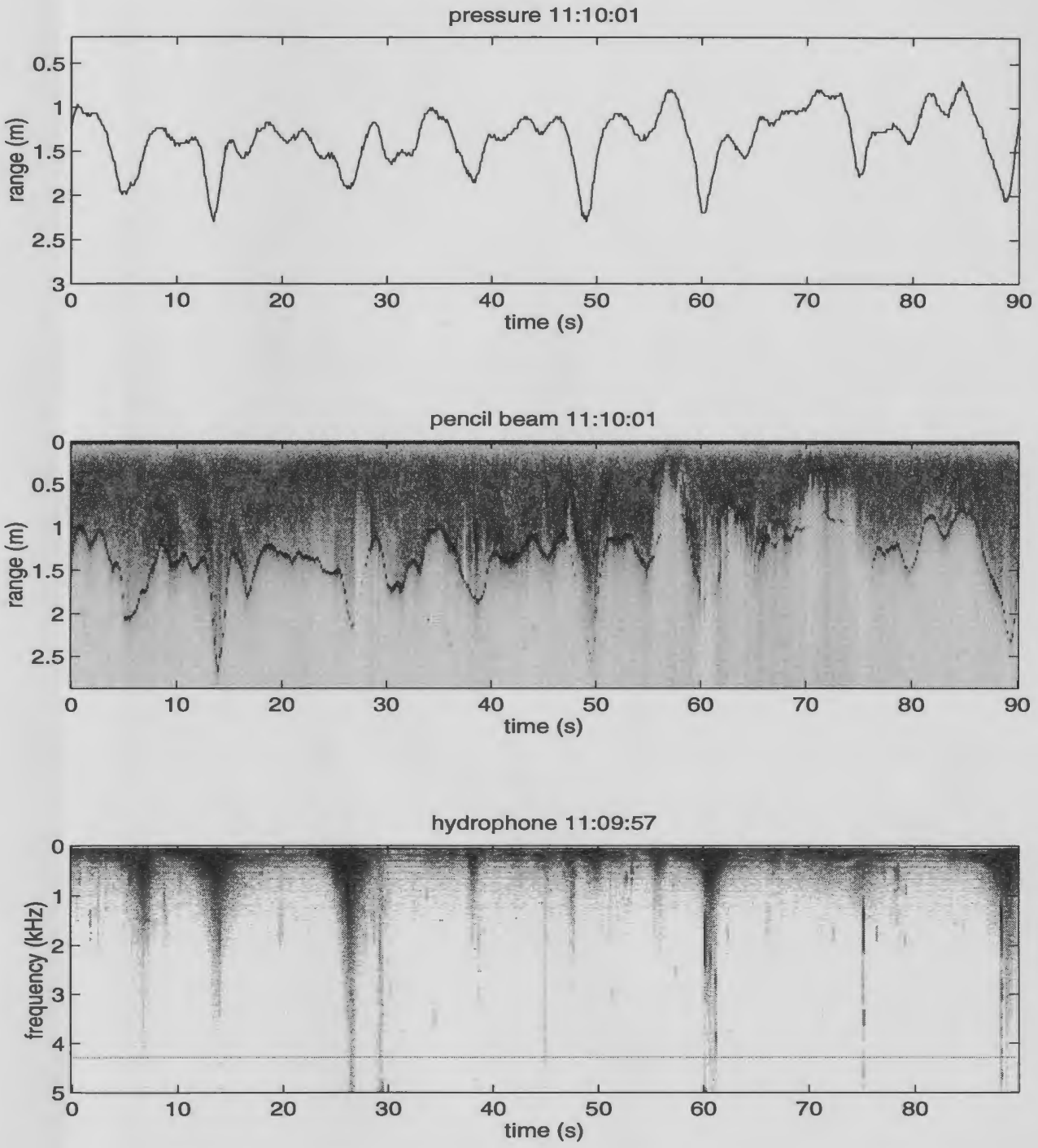

Figure 4.17: Time series taken from data from October 15 showing the pressure (top), the acoustic backscatter from the pencil beam (middle) and the spectra recorded from the hydrophone (bottom).

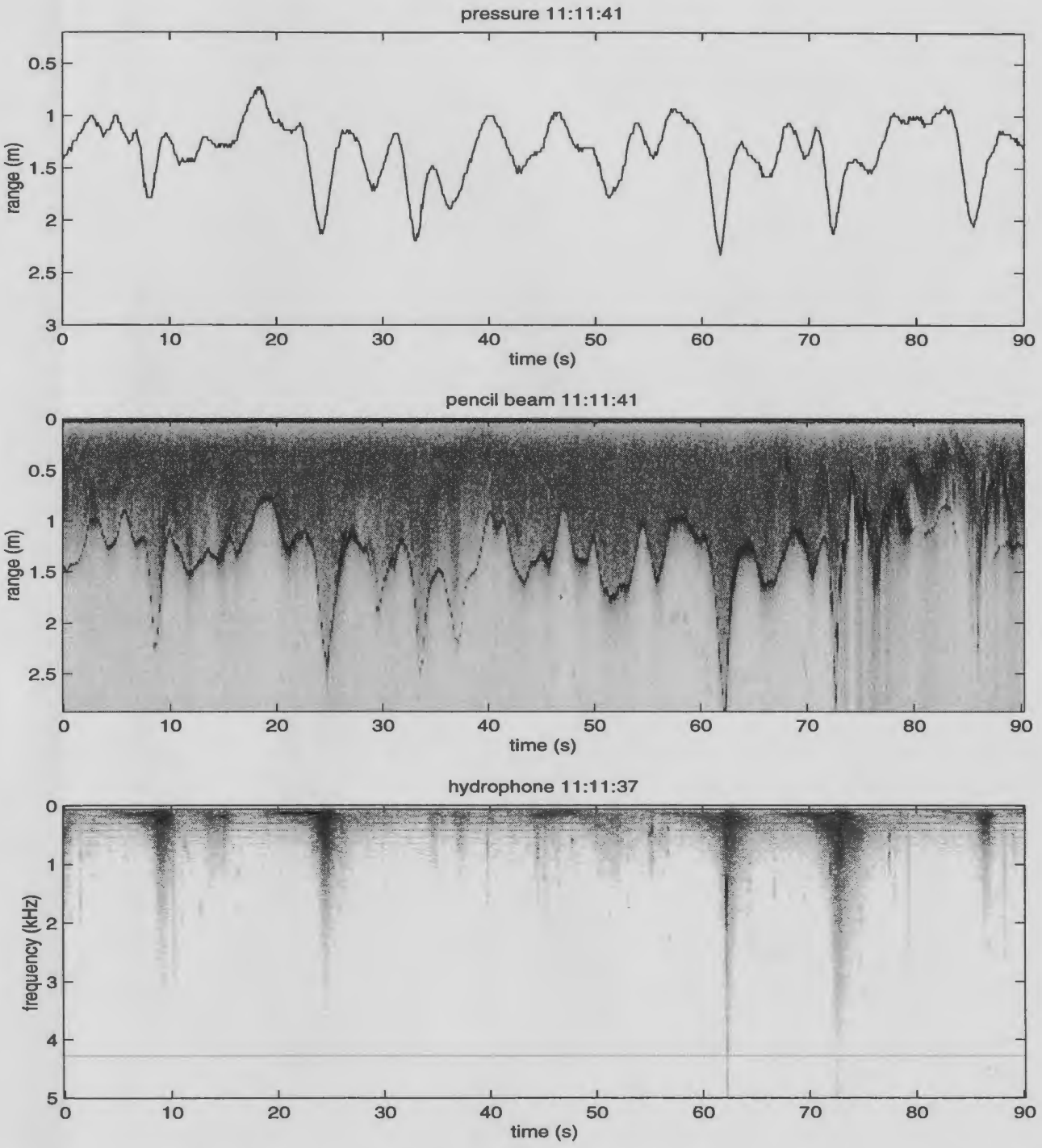

Figure 4.18: Time series taken from data from October 15 showing the pressure (top), the acoustic backscatter from the pencil beam (middle) and the spectra recorded from the hydrophone (bottom).

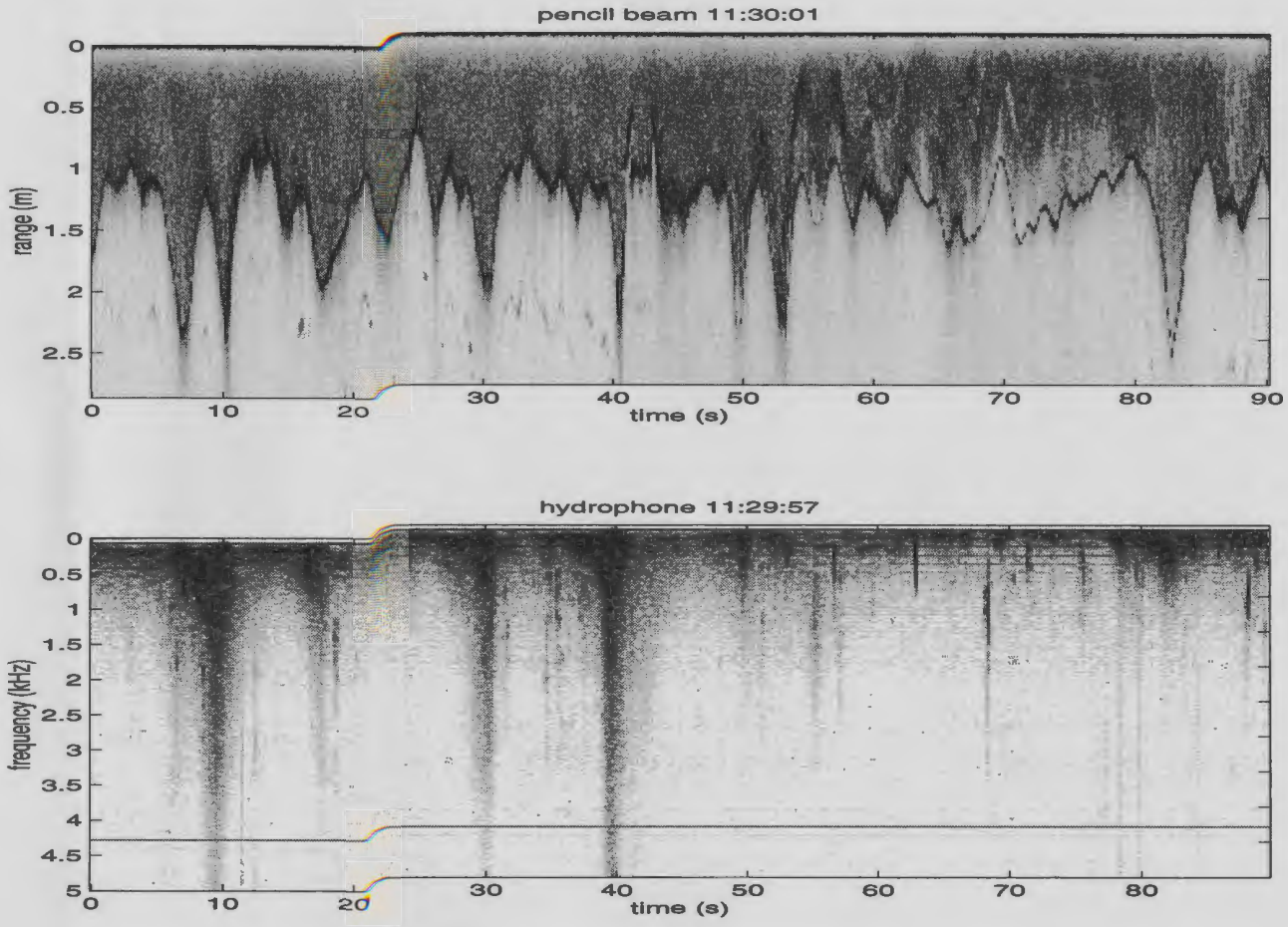

Figure 4.19: Time series taken from data from October 15 showing the acoustic backscatter from the pencil beam (top) and the spectra recorded from the hydrophone (bottom).

Comparison of the breaking events in Figures 4.12 to 4.19 with the wave height data from the pressure sensor and pencil beam sonar indicates that these events are not necessarily correlated with the passage of high waves. High waves, in some instances the highest waves in the record, need not produce much noise: for example, Figure 4.12 at 67 seconds; 4.13 at at 4 seconds; 4.14 at 22 seconds; 4.15 at 6 seconds; 4.16 at 30 seconds; 4.17 at 50 seconds; 4.18 at 33 seconds; and 4.19 at 53 seconds. Observation of the corresponding video indicates that these waves are not breaking as they pass over the hydrophone location. The absence of signal response in these figures to the passage of non-breaking waves, in particular high waves, suggests that the flow noise, discussed in section 4.2.3, is not a problem in these data.

Occurrences of spectral events are, however, correlated with wave crests in the pressure and sonar data. The overwater video confirms that these events correspond to the passage of breaking waves at the hydrophone location. Wave breaking at the sonar location is often suggested in the sonar data by the presence of bubble clouds which may be indicated by the dark patches underneath the waves or through obscuring of the water surface. In Figure 4.16, there is no sign of breaking in the pencil beam data for the entire record, yet distinct spectral events at 61 and 71 seconds in the hydrophone data suggest wave breaking at the hydrophone location. The corresponding video of the sea surface shows that both noise events are associated

with breaking waves at the hydrophone which finished breaking by the time they reached the sonar location. The distance between the 2 sensors means that wave breaking at one location does not imply wave breaking at the other.

The absence of sound generated by plunging waves on the bar and on the shore is also notable in Figure 4.16. Observation of the video shows that the sequence of waves, some of which are substantially high (about a metre in height), shown at 30, 40, 44, 51, 55, 61 and 71 seconds in Figure 4.16, initially broke on the bar at times corresponding respectively to 13, 22, 27, 36, 40, 44, and 55 seconds in Figure 4.16. There is no evidence in the spectra at these times of sound generated by the plunging waves on the bar. Waves which occur in Figure 4.16 before 30 seconds broke on the bar before the start of this time series. These times are summarized in Table 4.1.

Table 4.1: Times at which waves in Figure 4.16 break on the bar, and then appear at the hydrophone in Figure 4.16.

break on bar	break times in 4.16	reach hydrophone	hydrophone times in 4.16
11:11:19	-	11:11:36	10s
11:11:25	-	11:11:41	15s
11:11:39	13s	11:11:56	30s
11:11:48	22s	11:12:06	40s
11:11:53	27s	11:12:10	44s
11:12:02	36s	11:12:17	51s
11:12:06	40s	11:12:21	55s
11:12:10	44s	11:12:27	61s
11:12:21	55s	11:12:37	71s

The items discussed in this subsection (4.3.1) are consistent with the association between noise events and the passage of breaking waves over the hydrophone inferred from the overwater video, i.e. noise events detected by the hydrophone are mainly due to local breaking.

4.3.2 Bubble Screening

In the data presented, the restricted listening radius of the hydrophone may be explained by bubble screening effects. This screening is particularly apparent during the peak storm periods (e.g. Figures 4.12 and 4.13) when the surf was more energetic, probably creating a fairly constant background bubble population which absorbs and scatters acoustic radiation. The effects of bubble screening are also evident in Figure 4.16. For the interval between 0 and 55 seconds, there are no waves breaking directly above the hydrophone. However, as described earlier, the video indicates that waves are plunging on the bar in this interval and there is no evidence in the spectra that the hydrophone detects these events. A similar period of no breaking at the hydrophone occurs in Figure 4.14 in the interval of 10 to 60 seconds.

4.3.3 Breaking Wave Signature

In the results presented, the breaking events detected by the hydrophone are, in nearly all cases, from breakers which had plunged on the bar and continued breaking as spilling breakers as they propagated shoreward. The discreteness of the events implies that the nature of the sound production of an individual breaker may be studied.

When a wave plunges on a bar, bubbles are entrained mainly through 2 processes. First, as the crest of the wave overturns onto the forward slope of the wave it engulfs a cylindrical volume of air which is immediately broken up into a plume of bubbles. The second process is the entrainment of bubbles with the plunging jet impacting and penetrating the front face of the wave. This strong downward jet pushes up a turbulent mass of water which sustains the breaking through the mixing of air from above with water from below. Kolaini and Crum (1994) describe a large eddy (counter-clockwise for a wave travelling from right to left) which forms from the opposing directions of the downward jet and water pushed up into the cylindrical cavity region created by the plunging crest. This eddy is a possible mechanism for detachment of the bubble plume from the rest of the breaking wave and may transport the cloud to depths on the order of the wave height. If the wave continues breaking

with enough energy, a series of cylindrical plumes, or underwater rollers, may be created (Papanicolaou and Raichlen, 1988) which are driven down by vorticity and left behind as the wave propagates shoreward. These cylindrical clouds are thought to be likely candidates for low frequency collective oscillations and possibly contribute to the observed low frequencies in the noise events presented in this section.

After the initial plunging break of the wave on the bar, the wave is transformed into a bore-like spilling breaker which is characterized by a turbulent plume of air bubbles and water which rides on the forward face of the wave (Fredsoe and Deigaard, 1992). Bubbles are entrained beneath the surface of the wave by the turbulent flow created by the shear between the wave motion and the motion in the surface roller, and by vorticity. Loewen and Melville (1994) suggest that, for energetic spilling breakers, the layer of bubbles left in the wake of the wave may also oscillate collectively and contribute to low frequency emissions (although this has not been observed). They also suggest that energetic breakers may create significant numbers of larger bubbles (with radii on the order of a centimeter), with resonant frequencies in the neighbourhood of 500 Hz, and that there may be, in fact, a frequency region where both collective oscillations and individual bubble resonances contribute significantly. The above are other possible explanations for the intense low frequencies observed in the spectral events.

As previously described, the gradual increase in intensities, at the start of a noise event, begins at low frequencies and continues to higher frequencies as the breaking crest approaches the hydrophone. The event durations are comparable to the wave period and, from the video observations and the data in Figures 4.12-4.19, begin approximately under the trough ahead of the advancing wave crest. For 7-10 second waves, the crest at this point is 16-23 m away. The low frequency sounds detected by the hydrophone may be the result of some combination of the mechanisms mentioned above. These sounds, having a higher intensity and being dissipated less quickly than higher frequencies, are probably detected by the hydrophone first. As the wave passes overhead, the resonance of individual bubbles at kilohertz frequencies may be detected by the hydrophone. The rapid decay in intensities at all frequencies is most likely due to the bubble screening effect mentioned earlier. Breaking waves leave a trail of bubbly water which absorbs and scatters the sound of the breaking.

4.3.4 Breaking Frequency

As presented in the previous section, periods of energetic breaking in the surf zone reduce the scope of listening of the hydrophone through the screening effect of bubbles. This allows the identification of individual breaking waves passing over the hy-

drophone and consequently the means of estimating the local wave breaking frequency. Given the importance of wave energy dissipation in the surf zone, this measurement may be valuable in the study of nearshore processes.

Method

In order to count waves breaking above the hydrophone, the hydrophone spectra for each 570 second run were averaged over three frequency bands: approximately from 200 to 500 Hz, 500 to 1000 Hz and 1 to 2 kHz, and smoothed with a 6-point running average. An example is shown in Figure 4.20. Since the most intense sound lies in the 200 to 500 Hz band (denoted Band1), a threshold level was determined for Band1 using the minimum value in the 570 second interval as a base value and adding an appropriate constant. This constant was determined by comparing Band1 levels with the occurrence of breaking waves above the hydrophone as observed in the video. Although, there are occasional problems with salt and rain on the camera lens reducing visibility, it is usually fairly obvious which waves are breaking above the hydrophone, and it is only in a few cases where the whitecaps are short-crested or very gently spilling that there is some ambiguity.

The occurrence of the discrete low frequency sounds (in the region of 200 Hz), discussed in section 4.2.3, is not a problem in most of the data from peak storm

periods from October 11 to 15. Waves in this period tended not to be as high as on October 19. and the discrete frequency signal does not vary as much from it's approximate 200 Hz mean and. therefore. little of it is included in the 200-500 Hz band average. However. to limit the likelihood that this discrete low frequency is counted as a breaking wave. another minimum amplitude is determined for Band2 (500 to 1000 Hz) using the same method which also helps to avoid counting breakers close to. but not above. the hydrophone. In other words. whenever the signal in Band1 rises above the threshold amplitude. it is counted as a breaker as long as the signal in Band2 rises above the Band2 threshold at the same time.

Comparison of Breaking Frequencies, Wave Statistics and the Tide

Breaking waves were counted during the course of 4 days (October 11. 12. 14. and 15) of energetic surf and compared with offshore significant wave height and period and with the change in the mean sea level and wave height at the pressure sensor. Pressure data were not available for the afternoon of October 14 and for the full day on October 15. In order to obtain better statistical stability of the breaking frequency estimates. three consecutive 570 second runs were considered and the three breaking frequencies, from these runs, averaged. Breaking frequencies calculated by changing the threshold by plus or minus 15 percent are shown in Figures 4.21-4.23

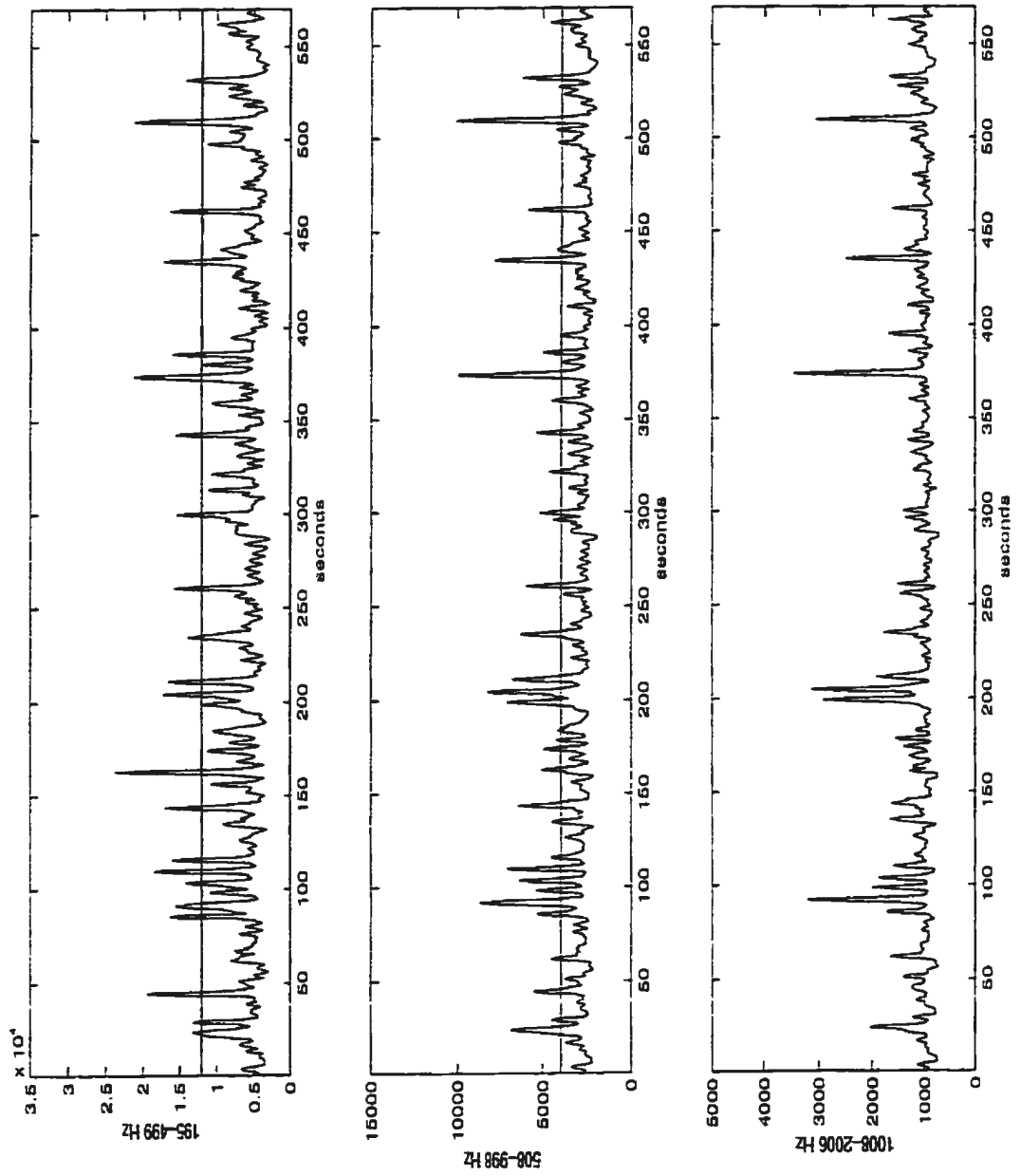

Figure 4.20: The top figure displays the smoothed 200-500 Hz band average (Band1) for a 570 second hydrophone spectral series from October 11, 13:00:00. The middle figure depicts the 500-1000 Hz band average (Band2), and the last depicts the 1-2 kHz band average (Band3).

for October 11, 12, and 14. These values could not be calculated for October 15 for technical reasons. While changing the magnitude of breakers somewhat, varying the threshold by 15 percent does not appear to change the overall pattern of breaking frequency throughout the course of a day. Note that the values of the 2 points at 13:15 and 14:15 on October 14 (Figure 4.23, top) are not reliable and are believed to be too large by between 0.5 and 0.8 (1/min). A large amount of static and unidentified sounds, counted as breakers, are present in the hydrophone data at these times. With the exception of the 2 points on the 14th, non-breaking events like those identified in Figure 4.6 (e.g. at 187 s) by their shorter duration than the breaking signals, alter the results of breaking frequency, by, on average, about +0.1 (1/min) with the unchanged threshold. During the peak storm periods from October 11 to 15, the non-breaking events could not be isolated effectively by considering peak widths alone. This complication is partly because of the variability of background levels and partly because the width of the peaks varies considerably. The solution of this problem is left for a future project.

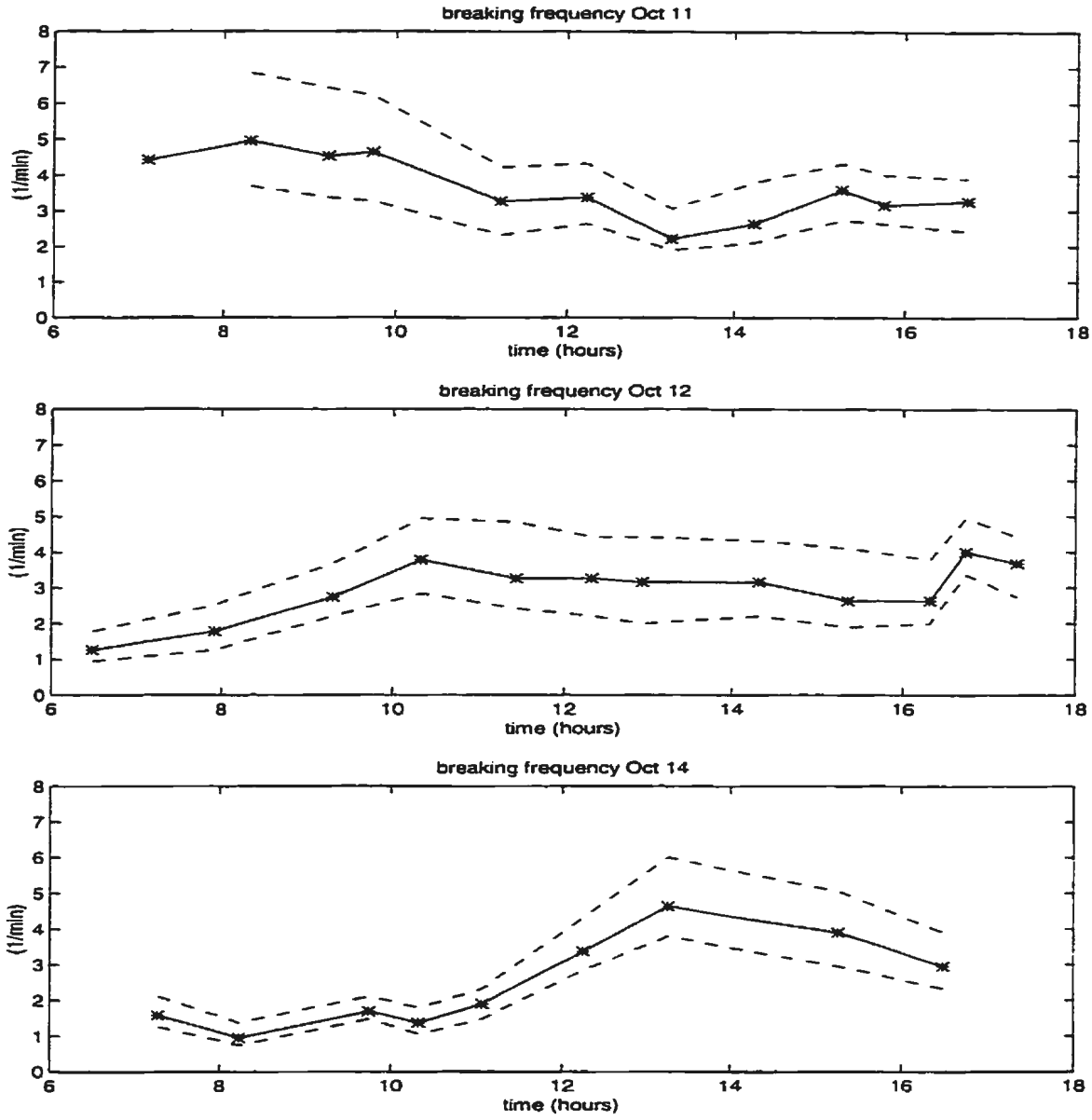

Figure 4.21: Wave breaking frequencies plotted against hour for October 11th. 12th. and 14th. Each point represents an average over 28.5 minutes. The 2 dotted lines in each plot represent breaking frequencies calculated using a 15 percent increase and decrease in the threshold amplitude .

Breaking frequencies are plotted, along with standard deviations, in Figures 4.22 to 4.25 for October 11, 12, 14, and 15, along with the offshore wave data, averaged over 3 hour intervals. Sea level changes were calculated as the mean of the pressure data over 30 minutes and the significant wave height calculated by multiplying the standard deviation by 4, which is based on a Rayleigh distribution for the wave height field (Horikawa, 1988). Underneath the breaking frequency plots are, respectively, the mean sea level above the pressure sensor which represents tidal changes, the offshore significant wave height, the wave height above the pressure sensor, and the peak offshore wave period which was determined from the peak in the offshore wave spectrum.

The correlation between the wave height inside the sand bar and the sea level changes is immediately noticeable in Figures 4.22 to 4.25. Waves break as they approach shallower water due to an instability which develops at the wave crest. From shallow water wave theory the phase speed of a wave in shallow water is depth dependent and is expressed by $c=\sqrt{gH}$. The instability at the crest can be represented by a smaller wavelength, yet still, shallow water wave. The depth of water at the wave crest is greater than that at the wave trough and so the phase speed of this instability will be greater than that of the wave. As the wave travels into shallower water the particles in the crest will start to overtake the particles in the trough, the

wave front steepens until eventually the wave breaks. This depth dependency means that deeper water can support taller waves. Once a wave has broken, the wave loses energy and the wave height decreases approximately linearly toward the shoreline. When sea level is low, waves are more likely to break on the offshore side of the bar meaning that they will lose more of their height before they reach the pressure sensor. As sea levels increase the waves travel closer to shore before they break thus increasing the height of waves observed at the pressure sensor.

From comparison of the breaking frequencies from October 11th, 12th, 14th, and 15th with the wave statistics plotted underneath (Figures 4.22-4.25), there appears to be a correlation with the offshore wave height. The tendancy of the breaking frequency to decrease through the day in Figure 4.22 (October 11th) follows the decrease in offshore wave height. Similarly, the breaking frequencies on October 12th, 14th, and 15th increase with offshore wave height at the beginning of the day and, for October 12th and 15th, they level off respectively around 10:00 and 14:00 with wave height. Waves break at a depth which is approximately 0.8 times their height (Fredsoe and Deigaard, 1992). The sand bar then acts as a filter allowing smaller waves to pass without breaking whereas the larger waves must break and then decrease in height. More waves are then likely to break on the bar and continue spilling over the hydrophone when the offshore wave height is greater.

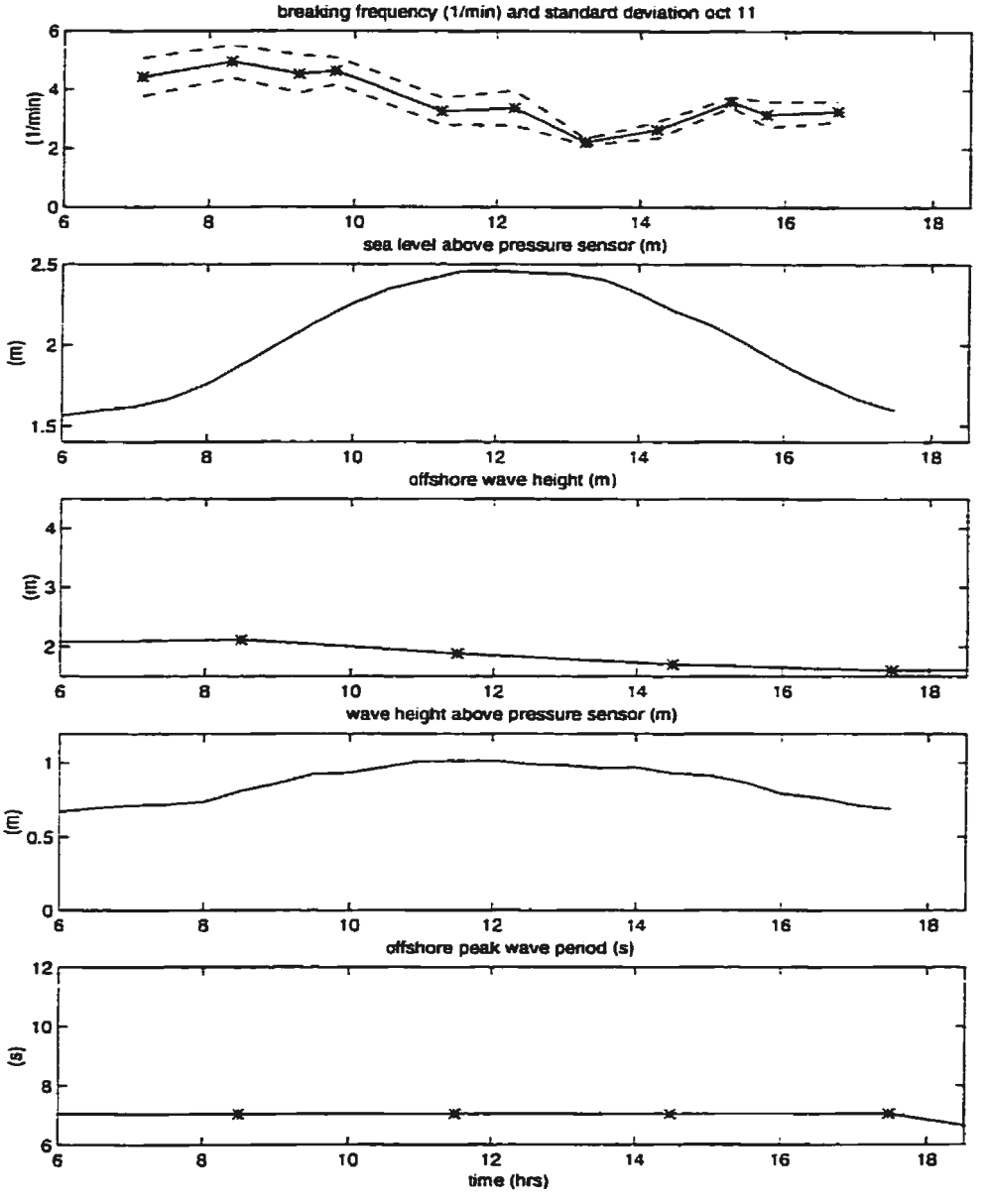

Figure 4.22: Wave breaking frequency plotted against hour for October 11. Each point represents an average over 28.5 minutes. Wave statistics are plotted below .

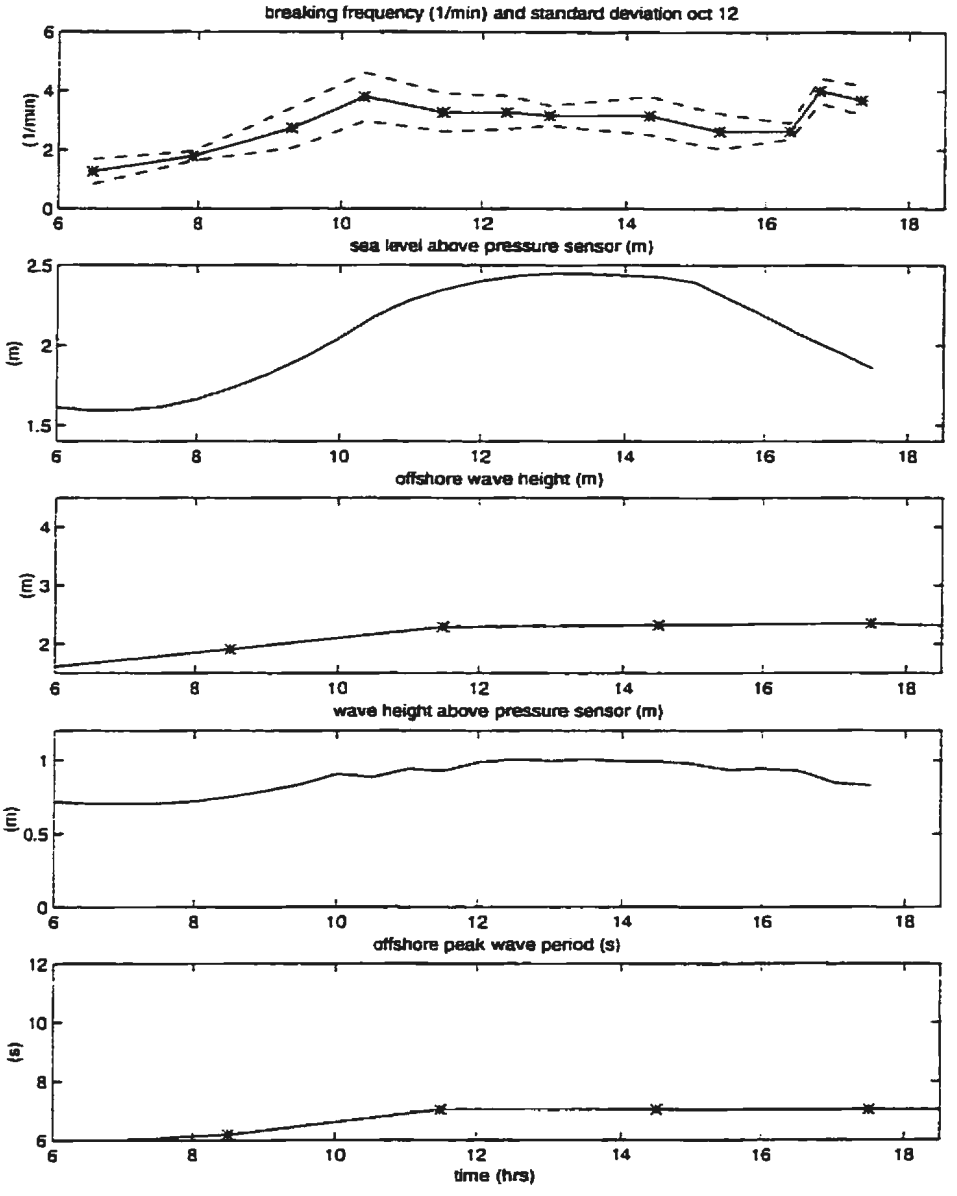

Figure 4.23: Wave breaking frequency plotted against hour for October 12. Each point represents an average over 28.5 minutes. Wave statistics are plotted below .

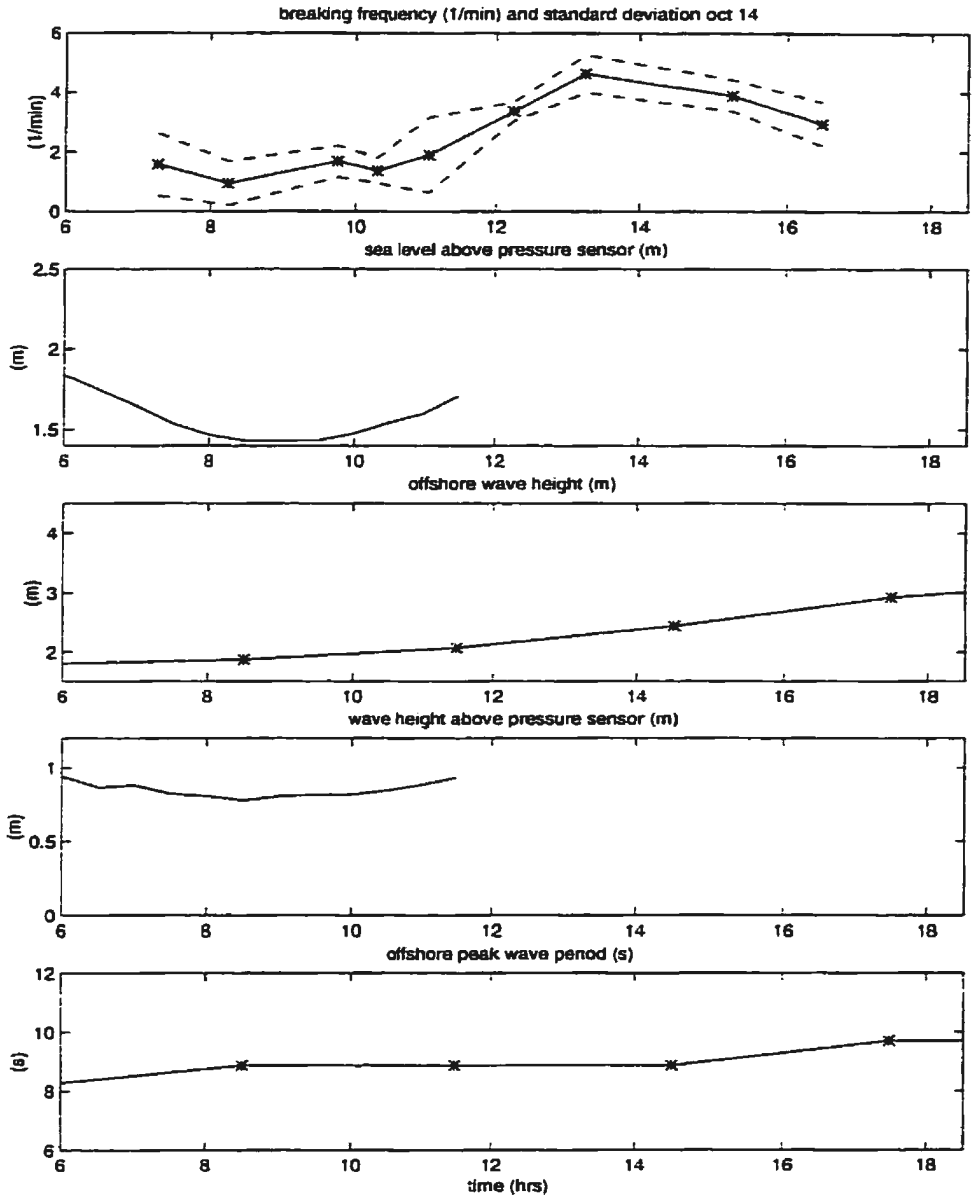

Figure 4.24: Wave breaking frequency plotted against hour for October 14. Each point represents an average over 28.5 minutes. Wave statistics are plotted below .

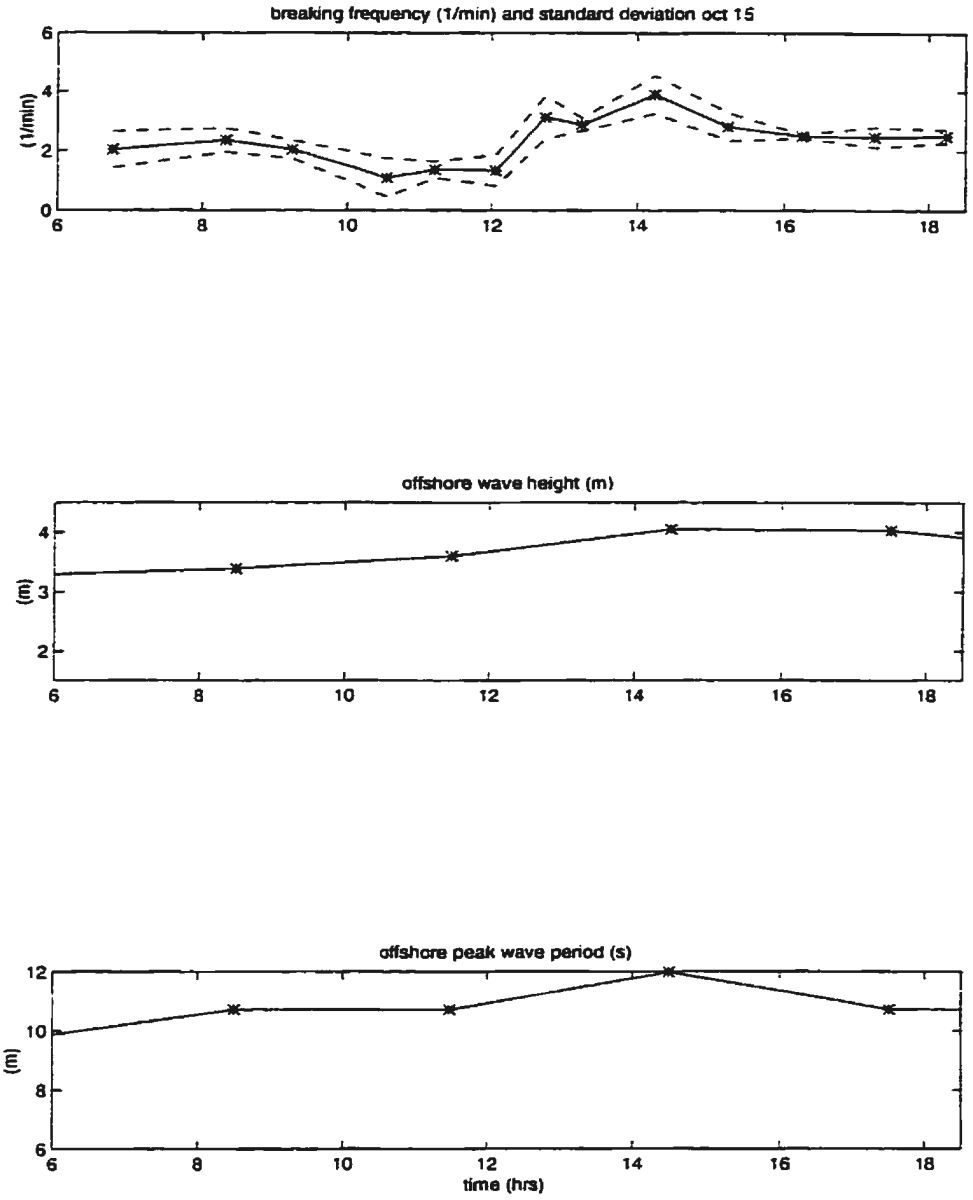

Figure 4.25: Wave breaking frequency plotted against hour for October 15. Each point represents an average over 28.5 minutes. Wave statistics are plotted below .

While there is a trend among the breaking frequency data to follow the offshore wave height, there are deviations which may in part be associated with tidal and offshore wave period variations. The data on the 11th and 12th, for example, exhibit a slight increase in breaking frequency towards the end of the day (Figures 4.22 and 4.23). These increases occur during intervals of relatively constant offshore wave period so they may be related to a decrease in the mean sea level. On October 11th, the breaking frequency appears to turn around and increase between 13:00 and 14:00 which is about the same time the sea level starts to drop. Likewise, on October 12th, the breaking frequency starts to increase between 15:00 and 16:00 at the same time the sea level decreases. This effect of sea level variations is also not unexpected since a decrease in water levels implies that more waves are likely to break on the bar, and thus, more breaking waves are detected by the hydrophone.

The variations in breaking frequency on October 14th and 15th (Figures 4.24 and 4.25) are less easily explained because of the simultaneous variations in offshore wave period, wave height and sea level. Although no pressure data were available, high tide occurred at about 15:30 on October 14th and low and high tide respectively at about 10:15 and 16:30 on October 15th. The decrease in breaking frequencies towards the end of October 14th and 15th (Figure 4.24 and 4.25) are possibly caused by a combination of an increase in mean sea level and an increase in offshore wave

period. The slightly lower breaking frequencies from 8:00 to 12:00 on the 15th (Figure 4.25) may also be related to the increase in wave period which occurs at the beginning of the 15th.

Variations in overall breaking frequencies between the days is not readily apparent despite the large increase in offshore wave height from the 11th to the 15th. This may be explained by the movement of the sand bar about 25 metres further offshore between the 11th and 14th. As the bar moves offshore, waves will break further offshore and hence they may stop breaking before they reach the hydrophone on more occasions than when the bar is closer to the shore.

Comparison with Breaking Frequency Estimates

The measured breaking frequencies in Figures 4.22 to 4.25 can be compared with estimates based on the depth of the bar, D_b, and the peak wave period, T_p. From profiles of the beach, the minimum depth of the sand bar is known for each day and, from this, the minimum offshore wave height required for waves to break on the bar (H_{bo}) can be calculated (Fredsoe and Deigaard, 1992).

$$H_{bo} = (\frac{4\pi}{g})^{1/2}(1.25g)^{1/4}\frac{(0.8D_b)^{5/4}}{T_p^{1/2}} \tag{4.1}$$

Assuming a Rayleigh distribution in the wave height field, the mean of the highest one third defines the significant wave height. If the offshore significant wave height, H_o, is equal to H_{bo}, then we can estimate that approximately one third of the waves, represented by the significant wave height, will be high enough to break on the bar. The estimated breaking frequency for waves of height H_{bo} is then one third the wave frequency or 60/wave period/3 (1/min). These variables: depth of bar, H_{bo}, H_o, wave frequency (f_w), estimated breaking frequency (f_e) for waves of height H_{bo}, and the measured breaking frequency (f_m), are summarized for each day (October 11th, 12th, 14th, 15th) at low, mid and high tide, in Tables 4.2 to 4.5.

Table 4.2: October 11th: depth of bar (D_b), offshore wave height required for breaking on the bar (H_{bo}), offshore significant wave height (H_o), wave frequency (f_w), estimated breaking frequency for waves of height H_{bo} (f_e), and the measured breaking frequency (f_m), are summarized at low, mid and high tide.

	low tide	mid-tide	high tide	mid-tide
D_b (m)	1.2	1.7	2.2	1.7
H_{bo} (m)	0.76	1.17	1.62	1.17
H_o (m)	2.07	2.11	1.88	1.70
f_w (1/s)	8.52	8.52	8.52	8.52
f_e (1/s)	2.84	2.84	2.84	2.84
f_m (1/s)	~4.5	~4.5	~3.3	~3.3

Table 4.3: October 12: depth of bar (D_b), offshore wave height required for breaking on the bar (H_{bo}), offshore significant wave height (H_o), wave frequency (f_w), estimated breaking frequency for waves of height H_{bo} (f_e), and the measured breaking frequency (f_m), are summarized at low, mid and high tide.

	low tide	mid-tide	high tide	mid-tide
D_b (m)	1.2	1.7	2.2	1.7
H_{bo} (m)	0.82	1.21	1.62	1.17
H_o (m)	1.70	1.91	2.30	2.30
f_w (1/s)	10.0	9.0	8.52	8.52
f_e (1/s)	3.3	3.0	2.84	2.84
f_m (1/s)	~1.5	~3.2	~3.1	~3

On all days and at all times, even for high tides, the offshore significant wave heights are greater than the minimum wave height required for waves to break on the bar (H_{bo}). All but 3 of the times (low, mid, high tides), have a breaking frequency which is higher (by about 0.2 to 1.7 breakers per min.) than that estimated. This discrepancy is expected since the significant wave heights, H_o, are higher than H_{bo}. The 3 times where the breaking frequency is lower (by about 0.5 to 2 breakers per min.) than that estimated, occur during low tides, which seems to suggest that the distance the waves travel before they stop breaking is important. At low tides in particular, waves will break on the offshore side of the bar, and, the further offshore that they break, the more likely it is that they will stop breaking before they reach the hydrophone.

Table 4.4: October 14: depth of bar (D_b), offshore wave height required for breaking on the bar (H_{bo}), offshore significant wave height (H_o), wave frequency (f_w), estimated breaking frequency for waves of height H_{bo} (f_e), and the measured breaking frequency (f_m), are summarized at low, mid and high tide.

	low tide	mid-tide	high tide
D_b (m)	1.4	1.9	2.4
H_{bo} (m)	0.82	1.20	1.58
H_o (m)	1.87	2.07	2.44
f_w (1/s)	6.76	6.76	6.40
f_e (1/s)	2.25	2.25	2.15
f_m (1/s)	~1.3	~3.3	~3.9

Table 4.5: October 15: depth of bar (D_b), offshore wave height required for breaking on the bar (H_{bo}), offshore significant wave height (H_o), wave frequency (f_w), estimated breaking frequency for waves of height H_{bo} (f_e), and the measured breaking frequency (f_m), are summarized at low, mid and high tide.

	low tide	mid-tide	high tide
D_b (m)	1.4	1.9	2.4
H_{bo} (m)	0.75	1.06	1.42
H_o (m)	3.60	3.80	4.05
f_w (1/s)	5.60	5.30	5.30
f_e (1/s)	1.87	1.77	1.77
f_m (1/s)	~1.3	~3.0	~2.4

Chapter 5

Summary & Conclusions

The subject of this thesis is the noise generated by breaking waves in the surf zone. In general, the sound field in shallow water is the net result of complex interactions of the sound with the sea floor and sea surface, sound speed profile variations with depth and distance, and multiple sound sources. From the results presented here, it appears that the nature of the energetic surf may reduce this complexity somewhat by limiting the listening radius. It is suggested that bubble clouds produced by breaking waves screen out sounds from distant sources, and this may be enhanced by trapping the sound through upward refraction into the upper bubbly layer of water where the sound is dissipated more quickly.

The location of the hydrophone in the trough between the sand bar and the

shore was useful. Waves were usually of plunging type on the sand bar and propagated toward the hydrophone as spilling breakers. Study of the ambient spectrum during periods of energetic breaking has revealed distinct broad band events associated mainly with the passage of individual breaking waves over the hydrophone. The events are preceded and followed by intervals of comparitive silence. During a breaking event. the ambient noise spectrum appears to evolve from increased intensities at a few hundred Hertz to increased intensities throughout the full spectrum. which then decay, often very rapidly. The low frequencies at the onset are associated with the approach of the breaker toward the hydrophone and may be generated by the collective oscillations of the bubble clouds being created in the breaking. As the wave passes over the hydrophone. plumes of bubbles left in the wake scatter and absorb the sound of the breaking. It is thought that this injection of bubbles may be the cause of the abrupt decrease in noise levels at all frequencies after the passage of a breaker. Narrow band pulses in the spectra. appearing as dark points in the spectral images. are thought to be caused by individual bubbles entrained near the hydrophone. Inspection of the voltage data at these pulses displays the distinct signature of an oscillating bubble.

In heavy surf, the sound sources detected by the hydrophone appear to be confined to a region on the order of ten metres radius. This restricted listening radius

implies that the breaking frequency above the hydrophone can be determined simply by counting the noise events. Breaking frequencies estimated from the ambient noise spectra indicate the expected correlation between breaking frequency and offshore wave height, modulated by the tide, and influenced also by offshore wave period.

While the mechanisms associated with the sound generation by breaking waves are the subject of ongoing research, and further work is needed on other sources of ambient sound, the results presented in this thesis indicate that ambient noise measurements have considerable potential for studies of wave breaking in the surf zone.

References

Banner, M.L. and D.H. Cato, Physical Mechanisms of Noise Generation by Breaking Waves - a Laboratory Study, in *Sea Surface Sound*, edited by B.R. Kerman (Kluwer Academic, Boston, 1988) pp. 429-435.

Bardyshev, V.I., N.G. Kozhelupova and V.I. Kryshnii, Study of Underwater noise Distributions in Inland Seas and Ocean Coastal Regions, *Sov. Phys. Acoust.*, 19(2), 95-96 (1973).

Bowen, A.J., The generation of longshore currents on a plane beach, *J. Mar. Res.*, 27, 206-215 (1969).

Carey, W.M. and M.P. Bradley, Low-frequency ocean surface noise surfaces, *J. Acoust Soc. Am. Suppl. 1* 78:S1-S2 (1985).

Carey, W.M. and D. Browning, Low Frequency Ocean Ambient Noise: Measurements and Theory, in *Sea Surface Sound*, edited by B.R. Kerman (Kluwer Academic, Boston, 1988) pp. 361-376.

Crighton, D.G. and J.E. Ffowcs Williams, Sound generation by turbulent two-phase flow, *J. Fluid Mech.* 36, 585-603 (1969).

Dupuis, H., J.P. Frangi and A. Weill, Comparison of wave breaking statistics using underwater noise and sea surface photographic analysis conducted under moderate wind speed conditions during the SOFIA/ASTEX experiment, *Ann. Geophysicae* 11, 960-969 (1993).

Farmer, D.M. and L. Ding, Coherent acoustical radiation from breaking waves, *J. Acoust Soc. Am.* 92(1), 397-402 (1992).

Farmer, D.M. and S. Vagle, On the determination of breaking surface wave distributions using ambient sound, *J. Geophys. Res.* 93(C4), 3591-3600 (1988a).

Farmer, D.M. and S. Vagle, Observations of high frequency ambient sound generated by wind, in *Sea Surface Sound*, edited by B.R. Kerman (Kluwer Academic, Boston, 1988b) pp. 403-415.

Fredsoe, J. and R. Deigaard 1992, Mechanics on Coastal Sediment Transport, World Scientific Publishing Co. Pte. Ltd., Singapore, 369 pp.

Gill, A.E. 1982. Atmosphere-Ocean Dynamics, Academic Press, New York, N.Y., 662 pp.

Hollett, R.D., Observations of underwater sound at frequencies below 1500 Hz from breaking waves at sea, *J. Acoust Soc. Am.* 95(1), 165-170 (1994).

Hollett, R.D. and R.M. Heitmeyer. Noise Generation by Bubbles Formed in Breaking Waves. in *Sea Surface Sound*, edited by B.R. Kerman (Kluwer Academic, Boston, 1988) pp. 449-461.

Horikawa, K. (Ed.), Nearshore Dynamics and Coastal Processes: Theory, Measurement, and Predictive Models, University of Tokyo Press, 1988.

Kerman, B.R., Underwater sound generation by breaking wind waves. *J. Acoust. Soc. Am.* 75(1), 149-165 (1984).

Knudsen, V.O., R.S. Alford, and J.W. Emling, Underwater ambient noise. *J. Mar. Res.* 7, 410-429 (1948).

Kolaini, A.R. and L.A. Crum, Observations of underwater sound from laboratory breaking waves and the implications concerning ambient noise in the ocean. *J. Acoust Soc. Am.* 96(3), 1755-1765 (1994).

Kolaini, A.R., R.A. Roy, L.A. Crum, and Y. Mao, Low-frequency underwater sound generation by impacting transient cylindrical water jets. *J. Acoust Soc. Am.* 94(5), 2809-2819 (1993).

Kundu, P.K., Fluid Mechanics, Academic Press (1990).

Leighton, T.G., *The Acoustic Bubble*, Academic Press Limited, London, 1994.

Long, C.E., Storm Evolution of Directional Seas in Shallow water, US Army Corps of Engineers, Technical Report CERC-94-2, 1994.

Longuet-Higgins, M.S., An analytic model of sound produced by raindrops. *J. Fluid Mech.* 214, 395-410 (1990a).

Longuet-Higgins, M.S., Bubble noise spectra. *J. Acoust Soc. Am.* 87(2), 652-661 (1990b)

Loewen, M.R. and W.K. Melville, An experimental investigation of the collective oscillations of bubble plumes entrained by breaking waves. *J. Acoust. Soc. Am.* 95(3), 1329-1343 (1994).

Lu, N.Q., A. Prosperetti, and S.W. Yoon, Underwater noise emissions from bubble clouds. *IEEE J. Ocean Eng.* 15(4), 275-281 (1990).

McConnell, S.O., M.P. Schilt, and J.G. Dworski, Ambient noise measurements from 100 Hz to 80 kHz in an Alaskan fjord. *J. Acoust Soc. Am.* 91(4), 1990-2003 (1992).

Medwin, H. and M.M. Beaky, Bubble sources of the Knudsen sea noise spectra. *J. Acoust Soc. Am.* 86(3), 1124-1130 (1989).

Medwin, H. and A.C. Daniel Jr., Acoustical measurements of bubble production by spilling breakers. *J. Acoust Soc. Am.* 88(1), 408-412 (1990).

Minnaert, M., On musical air-bubbles and sounds of running water. *Phil. Mag.* 16, 235-248 (1933).

Monahan, E.C. and M. Lu, Acoustically relevant bubble assemblages and their dependence on meteorological parameters. *IEEE J. Ocean Eng.* 15(4), 340-349 (1990).

Oguz, H.N., A theoretical study of low-frequency oceanic ambient noise. *J. Acoust. Soc. Am.* 95(4), 1895-1912 (1994).

Papanicolaou, P. and F. Raichlen, Wave and Bubble Characteristics in the Surf Zone. in *Sea Surface Sound*, edited by B.R. Kerman (Kluwer Academic, Boston, 1988), pp. 97-109.

Prosperetti, A., Bubble-related ambient noise in the ocean. *J. Acoust. Soc. Am.* 84(3), 1042-1054 (1988).

Prosperetti, A., Bubble dynamics in oceanic ambient noise in *Sea Surface Sound*, edited by B.R. Kerman (Kluwer Academic, Boston, 1988) pp. 151-172.

Pumphrey, H.C. and L.A. Crum, Acoustic Emissions Associated with Drop Impacts. in *Sea Surface Sound*, edited by B.R. Kerman (Kluwer Academic, Boston, 1988) pp. 463-483.

Pumphrey, H.C. and J.E. Ffowcs Williams, Bubbles as sources of ambient noise. *IEEE J. Ocean Eng.* 15(4), 268-274 (1990).

Stewart, M.S., Shallow Water Ambient Noise Caused by Breaking Waves in the Surf Zone. M.Sc. Thesis, Naval Postgraduate School, Monterey, California (1994).

Updegraff, G.E. and V.C. Anderson, Bubble noise and wavelet spills recorded 1 m below the ocean surface. *J. Acoust. Soc. Am.* 89(5), 2264-2279 (1991).

Wenz, G.M. Acoustic ambient noise in the ocean: Spectra and sources. *J. Acoust. Soc. Am.* 34(12), 1936-1956 (1962).

Wilson, O.B., Jr., S.N. Wolf and F. Ingenito, Measurements of acoustic ambient noise in shallow water due to breaking surf. *J. Acoust. Soc. Am.* 78(1), 190-195 (1985).

Yoon, S.W., L.A. Crum, A. Prosperetti, and N.Q. Lu, An investigation of the collective oscillations of a bubble cloud. *J. Acoust. Soc. Am.* 89(2), 700-706 (1991).